eLife

Reviewed Preprint
v1 • June 23, 2026
Not revised

For correspondence:
hughes@biochem.utah.edu

Competing interests: No competing interests declared

Funding: See page 24

Reviewing editor: Luke Wiseman, Scripps Research Institute, United States

Proteolytic remodeling by Yme1 enables mitochondrial-derived compartment formation

Sai Sangeetha Balasubramaniam[1], Amy E Curtis[1], Jonathan R Friedman[2], Adam L Hughes[1]

[1]Department of Biochemistry, University of Utah School of Medicine, Salt Lake City, United States • [2]Department of Cell Biology, University of Texas Southwestern Medical Center, Dallas, United States

eLife Assessment

This **valuable** study demonstrates that the inner membrane protease YME1 contributes to the formation of mitochondrial-derived compartments in yeast through the modulation of both the lipid transporter UPS2 and the MICOS complex. The evidence supporting this model is **solid**, although this manuscript could be improved by providing additional evidence supporting the independent roles for UPS2 and MICOS regulation in this process. This work will be of interest to cell biologists, biochemists, and geneticists interested in understanding the molecular basis of mitochondrial regulation and function.

https://doi.org/10.7554/eLife.111713.1.sa4

Abstract

Mitochondrial-derived compartments (MDCs) are remodeling domains that form from the outer mitochondrial membrane during metabolic and proteotoxic stress and selectively sequester hydrophobic membrane proteins. Although MDC formation depends on mitochondrial lipid composition and occurs at organelle contact sites, the molecular mechanisms that permit their biogenesis remain poorly defined. Here we identify the conserved inner mitochondrial membrane i-AAA protease Yme1 as a critical regulator of MDC formation. Loss of Yme1 blocks MDC biogenesis in response to multiple stressors, and this requirement depends on its proteolytic activity rather than secondary defects in mitochondrial morphology. Quantitative mitochondrial proteomics under MDC-inducing conditions revealed Yme1-dependent remodeling of lipid transfer proteins of the Ups family and components of the MICOS complex. Disruption of either pathway partially restores MDC formation in *yme1Δ* cells, while combined perturbation substantially bypasses the requirement for Yme1. Finally, Yme1 overexpression drives MDC formation in the absence of stress, although this activity remains constrained by metabolic conditions. Together, these findings support a model in which Yme1-dependent proteolysis relieves lipid- and MICOS-dependent constraints to permit MDC formation.

Introduction

Mitochondrial plasticity enables cells to adapt to fluctuating physiological and nutrient conditions, thereby preserving cellular homeostasis (Cogliati *et al*, 2016; Bahat & Gross, 2019) This adaptability arises from coordinated functional and structural remodeling of both the outer and inner mitochondrial membranes (Pfanner *et al*, 2019; Colina-Tenorio *et al*, 2020). Mitochondrial membrane remodeling is therefore central to these adaptations, integrating changes in membrane architecture, lipid composition, and protein content in response to diverse stressors (Yang *et al*, 2022; Klecker & Westermann, 2021). These processes occur across a spectrum ranging from selective protein turnover mediated by mitochondrial proteases to large-scale degradation of entire organelles (Ng *et al*, 2021; Suomalainen & Nunnari, 2024). For example, mitophagy eliminates damaged mitochondria in response to severe or sustained stress,

such as nutrient deprivation, hypoxia, mitochondrial poisons, or defects in protein import (Schuster & Okamoto, 2022; Abeliovich, 2023). In contrast, more selective remodeling pathways preserve mitochondrial integrity by removing or reorganizing specific components. These include mitochondrial-derived vesicles (MDVs), which form under steady-state conditions or during oxidative stress and encapsulate protein cargo from multiple mitochondrial subcompartments within membranes derived from the outer mitochondrial membrane or both mitochondrial membranes (Sugiura *et al*, 2014; Picca *et al*, 2023; König & McBride, 2024). Similarly, pathological perturbations, such as those observed during *Toxoplasma gondii* infection, remodel the outer mitochondrial membrane into large ring-shaped structures termed structures positive for the outer membrane (SPOTs), which incorporate specific OMM proteins while excluding intramitochondrial components (Li *et al*, 2022).

Among these pathways, a recently described mechanism of outer mitochondrial membrane remodeling is the mitochondrial-derived compartment (MDC) pathway (Hughes *et al*, 2016). MDCs are multilamellar structures that emerge from the outer mitochondrial membrane during metabolic and proteotoxic stress in budding yeast and mammalian cells (Schuler *et al*, 2020; Schuler *et al*, 2021; Wilson *et al*, 2024; Raghuram & Hughes, 2024). Under conditions such as elevated intracellular amino acid levels or disruptions in protein homeostasis, the outer mitochondrial membrane undergoes successive rounds of elongation and invagination to generate MDCs (Schuler *et al*, 2020; Wilson *et al*, 2024). Pharmacological perturbations that elevate intracellular amino acid pools in yeast, including inhibition of vacuolar amino acid storage with concanamycin A (ConcA) or translational inhibition with rapamycin (Rap) or cycloheximide (CHX), robustly induce MDC formation (Hughes *et al*, 2016; Schuler *et al*, 2021).

Upon formation, MDCs selectively sequester the mitochondrial import receptor Tom70 together with a defined subset of outer mitochondrial membrane proteins, while excluding proteins from other mitochondrial subcompartments (Hughes *et al*, 2016; Schuler *et al*, 2021; Wilson *et al*, 2024). These structures therefore represent specialized mitochondrial remodeling domains that capture and compartmentalize hydrophobic outer membrane cargo during metabolic and proteotoxic stress (Wilson *et al*, 2024; Raghuram & Hughes, 2024). MDCs arise through successive rounds of outer mitochondrial membrane elongation and invagination, generating multilamellar compartments composed exclusively of outer membrane (Wilson *et al*, 2024). Previous work, including an unbiased genome-wide genetic screen for regulators of MDC formation, identified mitochondrial lipid homeostasis as a critical determinant of this pathway (Xiao *et al*, 2024). In particular, mitochondrial lipid transfer proteins of the Ups family and components of the ER–mitochondria encounter structure (ERMES) were found to be required for MDC biogenesis, indicating that mitochondrial lipid composition and membrane organization play central roles in generating these compartments (English *et al*, 2020; Xiao *et al*, 2024). Despite these advances, the molecular mechanisms that drive MDC formation remain poorly understood, and it is still unclear how metabolic or proteotoxic stress is translated into the lipid and membrane remodeling events that produce these cargo-sequestering structures.

Among the candidates identified in this previous screen for MDC regulators was the conserved inner mitochondrial membrane i-AAA protease Yme1, an inner mitochondrial membrane (IMM)-localized mitochondrial protease known to regulate membrane protein turnover and mitochondrial membrane organization (Weber *et al*, 1996; Leonhard *et al*, 1999; Deshwal *et al*, 2020; Kan *et al*, 2024). Given the emerging importance of mitochondrial lipid composition and membrane architecture in MDC formation, we therefore investigated whether Yme1 contributes to MDC biogenesis.

In this study, we find that Yme1 proteolytic activity is required for MDC formation in response to multiple metabolic stress conditions that induce MDCs. Quantitative mitochondrial proteomics under MDC-inducing conditions revealed Yme1-dependent remodeling of lipid transfer proteins of the Ups family and components of the MICOS complex. Genetic perturbation of these pathways partially restores MDC formation in *yme1Δ* cells, while combined disruption substantially bypasses the requirement for Yme1. Together, these findings identify Yme1 proteolysis as a key regulator of

MDC biogenesis and support a model in which Yme1-dependent remodeling of mitochondrial lipid transfer and membrane-organizing complexes relieves constraints that otherwise limit MDC formation.

Results and discussion

Proteolytic activity of Yme1 is required for MDC formation

To investigate the potential role of Yme1 in the MDC pathway, we examined the impact of *YME1* deletion on MDC formation across several well-characterized MDC inducers. MDCs were quantified using a fluorescence microscopy assay in which MDCs appear as discrete Tom70-positive puncta that are enriched for outer mitochondrial membrane proteins while excluding inner mitochondrial membrane markers such as Tim50, thereby distinguishing them from the contiguous mitochondrial network (Hughes *et al*, 2016; Fig. 1A). Consistent with the preliminary results from our previous MDC screen, we found that deletion of *YME1* blocked MDC formation in response to a 2-hour exposure to Rap, ConcA, and CHX (Fig. 1A-B, Fig. S1A).

Cells lacking Yme1 exhibit aberrant mitochondrial morphology, a high rate of mitochondrial DNA escape, and growth defects on nonfermentable media (Thorsness & Fox, 1993; Weber *et al*, 1996). Because loss of *YME1* disrupts mitochondrial morphology, we asked whether the MDC defect in *yme1Δ* cells arises as a secondary consequence of these structural alterations. To test this, we examined whether restoring mitochondrial morphology rescues MDC formation in *yme1Δ* mutants. Expression of a mutant form of the proteasome component Rpt3 (P215L) has been reported to suppress certain growth defects and alleviate mitochondrial morphological abnormalities in cells lacking *YME1* (Campbell *et al* 1994; Francis & Thorsness, 2011). Consistent with previous observations, we found that strains expressing *pRPT3(P215L)* exhibited substantial recovery of mitochondrial morphology but still failed to form MDCs (Fig. 1C-D, Fig. S1B-D). Moreover, Rap treatment also restored mitochondrial morphology in *yme1Δ* mutants through an unknown mechanism despite MDCs remaining absent (Fig. S1E). To determine whether loss of mtDNA contributes to the MDC defect in *yme1Δ* mutants, we examined MDC formation in wild-type cells lacking mitochondrial DNA (rho⁰). We found that rho⁰ cells exhibited MDC formation even in the absence of stress, indicating that mtDNA is not required for MDC induction (Fig. S1F-G). Together, these results indicate that neither altered mitochondrial morphology nor loss of mtDNA accounts for the MDC defect observed in *yme1Δ* cells.

To test whether the protease activity of Yme1 is required for MDC formation, we generated *yme1Δ* strains ectopically expressing either wild-type Yme1 or a catalytically inactive mutant ($yme1^{E541Q}$) (Leonhard *et al*, 1999). Expression of wild-type Yme1 moderately restored MDC formation, whereas the protease mutant failed to rescue MDC formation in cells lacking *YME1* (Fig. 1E-F, Fig. S1H). Finally, we found that overexpression of wild-type Yme1 from a strong, constitutive GPD promoter, but not the catalytically inactive mutant, was sufficient to trigger MDC formation in in the absence of stress (Fig. 1G-H). These results indicate that elevated Yme1 levels can drive MDC formation in a manner dependent on its proteolytic activity Collectively, these data establish that Yme1 proteolytic activity is critical for MDC biogenesis.

MDC Induction Triggers Yme1-Dependent Changes in the Mitochondrial Proteome

Given that the proteolytic activity of Yme1 is required for MDC biogenesis, we hypothesized that Yme1-dependent remodeling of mitochondrial proteins may be important for regulation of this pathway. To identify potential candidates, we performed TMT-based quantitative proteomics on mitochondria isolated from wild-type and *yme1Δ* cells in the absence and presence of a two-hour Rap treatment. Proteomic profiling identified more than 4,000 proteins and revealed extensive remodeling of the mitochondrial proteome upon MDC induction in a Yme1-dependent manner. Quality control analyses, including principal component analysis and normalization across samples, confirmed robust separation of the experimental groups and successful dataset normalization (Fig. S2A-B).

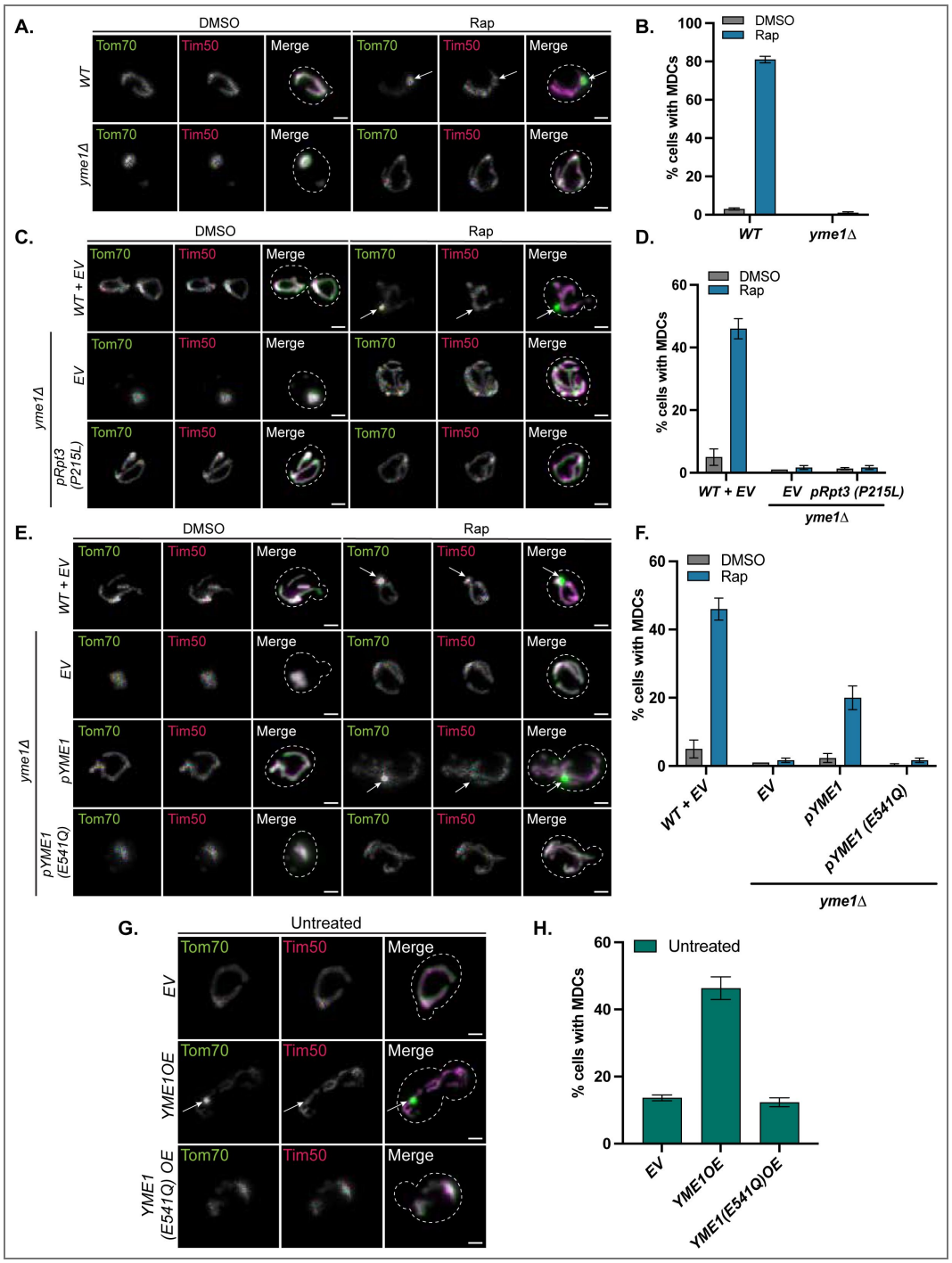

Figure 1. Proteolytic activity of Yme1 is required for MDC formation.

(A) Widefield images of wild-type and *yme1Δ* cells expressing Tom70-GFP and Tim50-mCherry treated with DMSO or Rap for 2 h. White arrows denote MDCs. Scale bar = 2 µm. (B) Quantification of (A) showing the percentage of cells with MDCs. Error bars represent the mean ± SE of three replicates, *n* ≥ 100 cells per replicate. (C) Widefield images of wild-type and *yme1Δ* cells endogenously tagged with Tom70-GFP and Tim50-mCherry expressing either *EV* or *pRS413-Rpt3 (P215L)* treated with DMSO or Rap for 2 h. White arrows denote MDCs. Scale bar = 2 µm. (D) Quantification of (C) showing the percentage of cells with MDCs. Error bars represent the mean ± SE of three replicates, *n* ≥ 100 cells per replicate. (E) Widefield images of wild-type and *yme1Δ* cells endogenously tagged with Tom70-GFP and Tim50-mCherry expressing either *EV*, *pRS413-Yme1*, or *pRS413-Yme1 (E541Q)* treated with DMSO or Rap for 2 h. White arrows denote MDCs. Scale bar = 2 µm. (F) Quantification of (E) showing the percentage of cells with MDCs. Error bars represent the mean ± SE of three replicates, *n* ≥ 100 cells per replicate. (G) Widefield images of yeast cells tagged with Tom70-GFP and Tim50-mCherry, constitutively overexpressing *YME1* (*YME1 OE*), the protease-dead mutant, *YME1(E541Q)*, or an empty vector (*EV*) control. White arrows denote MDCs. Scale bar = 2 µm. (H) Quantification of (G) showing the percentage of cells with MDCs. Error bars represent the mean ± SE of three replicates, *n* ≥ 100 cells per replicate.

To identify broader biological patterns within the dataset, we grouped proteins based on shared changes in abundance across conditions. Hierarchical clustering identified distinct functional groups encompassing mitochondrial protein import, membrane organization, metabolism, and lipid homeostasis, several of which have previously been linked to MDC biogenesis (Fig. 2A). Thus, MDC induction is accompanied by broad remodeling of mitochondrial pathways, and loss of Yme1 alters multiple protein groups likely relevant to MDC formation.

To identify the proteins most strongly affected by loss of Yme1 under MDC-inducing conditions that may be good candidates for MDC regulators, we next compared the Rap-treated wild-type and *yme1Δ* mitochondrial proteomes by volcano plot analysis (Fig. 2B). Among the most significantly elevated proteins in *yme1Δ* cells were Ups1 and Ups2, members of the conserved Ups/PRELID family of mitochondrial lipid transfer proteins that shuttle phospholipid precursors between mitochondrial membranes (Potting *et al*, 2010; Tamura *et al*, 2012; Connerth *et al*, 2012; Aaltonen *et al*, 2016; Tatsuta & Langer, 2017; MacVicar *et al*, 2019; Perea *et al*, 2023). In addition, several components of the MICOS complex (mitochondrial contact site and cristae organizing system) were also elevated (Schreiner *et al*, 2012; Li *et al*, 2016). MICOS is a conserved multiprotein complex located at crista junctions that maintains inner mitochondrial membrane architecture and coordinates membrane contact sites between mitochondrial subcompartments (Aaltonen *et al*, 2016; Cogliati *et al*, 2016; Huynen *et al*, 2016; Mukherjee *et al*, 2021). The elevated protein dataset also included proteins involved in mitochondrial protein import, including members of the small TIM chaperone complexes, which facilitate the transfer of hydrophobic precursor proteins across the intermembrane space (Koehler *et al*, 1998; Koehler, 1998; Baker *et al*, 2012; Spiller *et al*, 2015), and Pam17, a regulatory component of the mitochondrial inner membrane import motor that assists in translocation of proteins into the matrix (Van Der Laan *et al*, 2005; Schiller, 2009). Notably, many of these proteins reside within mitochondrial subcompartments accessible to Yme1 proteolysis, including the IMM and intermembrane space (IMS), and several are well-established Yme1-regulated substrates, including the Ups proteins. Together, these results show that loss of Yme1 alters the abundance of proteins across multiple mitochondrial pathways under MDC-inducing conditions, providing a pool of candidate regulators for further investigation.

Yme1 regulation of Ups2 contributes to MDC formation

To determine whether proteins elevated in *yme1Δ* cells might represent Yme1-regulated factors that influence MDC biogenesis, we next examined candidates emerging from the proteomic analysis. Because MDC formation is completely blocked in *yme1Δ* cells while several proteins accumulate under these conditions, we reasoned that elevation of these proteins might inhibit MDC formation or that their ongoing activity may normally act as a constraint on MDC biogenesis. Among the strongest candidates were the mitochondrial lipid transfer proteins Ups1 and Ups2, which were significantly elevated in Rap-treated *yme1Δ* cells (Fig. 2B). The Ups proteins regulate mitochondrial lipid composition by shuttling phospholipid precursors from the outer mitochondrial membrane to the inner mitochondrial membrane (Tamura *et al*, 2012; Connerth *et al*, 2012; Aaltonen *et al*, 2016). Ups1 transfers phosphatidic acid (PA) for downstream cardiolipin synthesis, whereas Ups2 transports phosphatidylserine (PS) to facilitate phosphatidylethanolamine (PE) production. Previous work has shown that Yme1 mediates Ups2 turnover, while Ups1 degradation can be regulated by both Yme1 and the metallopeptidase Atp23 (Potting *et al*, 2010; Tatsuta & Langer, 2017).

To test whether the changes observed in our proteomic analysis reflect Yme1-dependent regulation of Ups proteins, we examined Ups1 and Ups2 protein levels by immunoblotting. Consistent with the proteomics dataset, Ups1 and Ups2 steady-state levels declined in wild-type cells following Rap treatment but accumulated and remained elevated in *yme1Δ* mutants under the same conditions (Fig. 3A-D). These results confirm that Ups proteins are regulated by Yme1 and that their abundance decreases under MDC-inducing conditions in a Yme1-dependent manner.

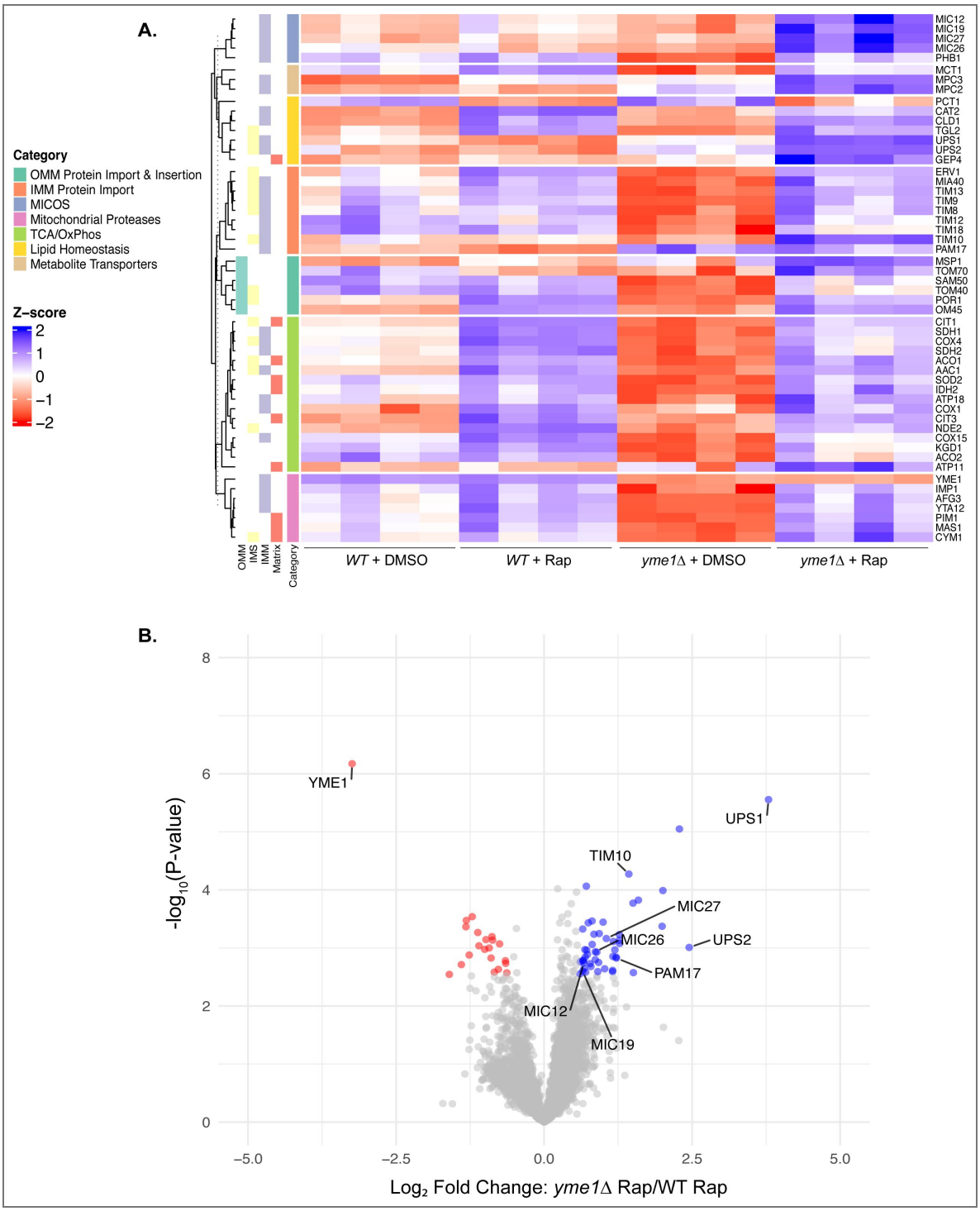

Figure 2. MDC Inducer Rapamycin triggers Yme1-dependent changes in the mitochondrial proteome.

(A) Clustered heatmap showing *Z*-scores of select mitochondrial proteins in wild-type and *yme1Δ* cells treated with DMSO or Rap for 2 h (n = 4), with corresponding mitochondrial subcategories indicated on the left. Proteins were categorized by GO Biological Processes (GO: BP) and manual annotation. Blue indicates upregulated proteins; red indicates downregulated proteins. (B) Volcano plot analysis of differentially expressed proteins in *yme1Δ* cells compared with wild-type cells following Rap treatment for 2 h (n = 4). Mitochondrial proteins enriched in *yme1Δ* cells are highlighted in blue and represent potential Yme1 substrates; red indicates downregulated proteins.

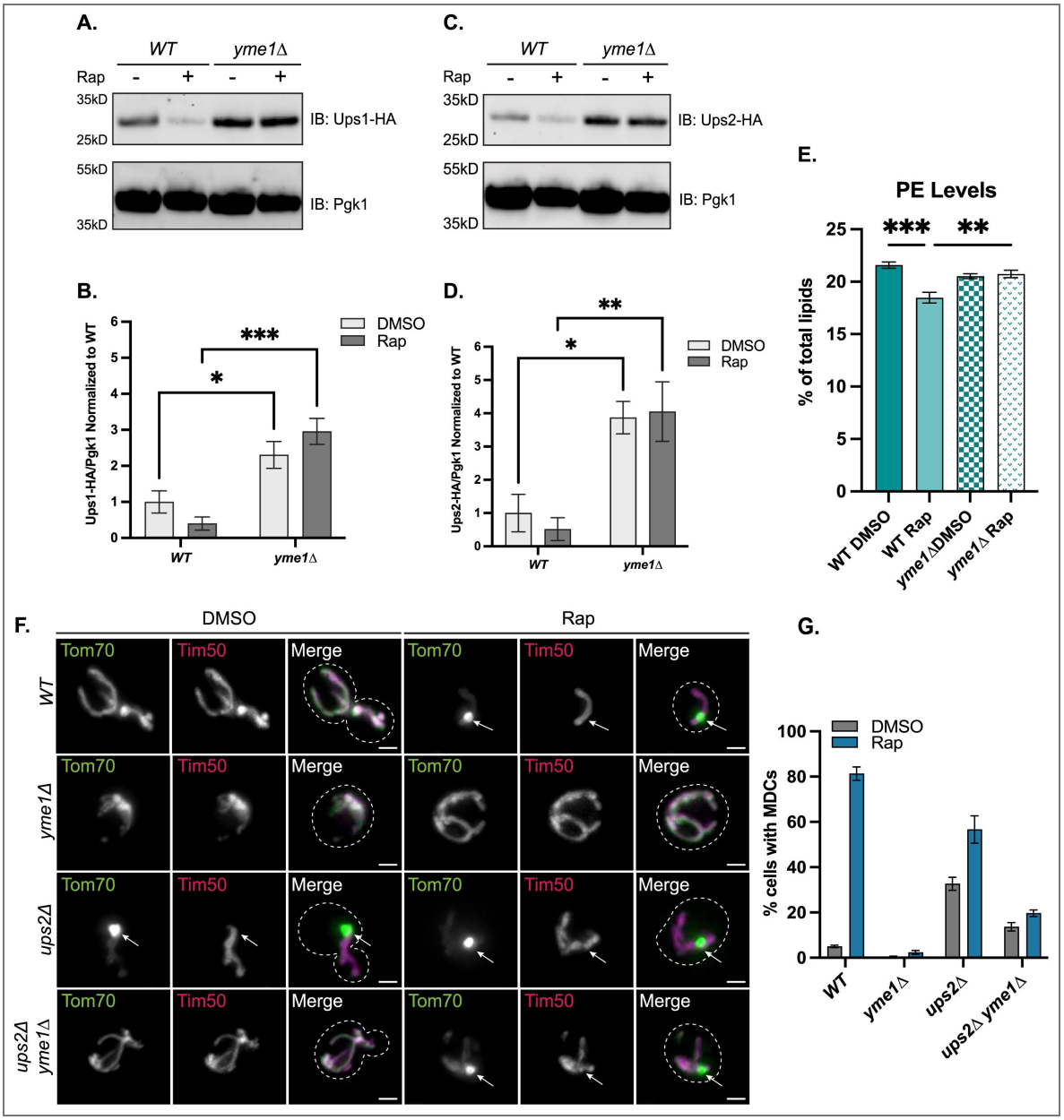

Figure 3. Yme1 regulation of Ups2 contributes to MDC formation.

(A) Immunoblot analysis of whole-cell lysates from yeast expressing endogenously tagged Ups1-HA, treated with DMSO or Rap for 2 h. Blots were probed with anti-HA; Pgk1 served as a loading control. Representative of n = 3 independent experiments. (B) Quantification of (A) wherein Ups1-HA levels were normalized to the corresponding Pgk1 signal and then normalized to *EV* cells treated with DMSO (n = 3). Statistical significance was determined by two-way ANOVA (*p ≤ 0.05, ***p ≤ 0.001). (C) Immunoblot analysis of whole-cell lysates from yeast expressing endogenously tagged Ups2-HA, treated with DMSO or Rap for 2 h. Blots were probed with anti-HA; Pgk1 served as a loading control. Representative of n = 3 independent experiments. (D) Quantification of (C) wherein Ups2-HA levels were normalized to the corresponding Pgk1 signal and then normalized to *EV* cells treated with DMSO (n = 3). Statistical significance was determined by two-way ANOVA (*p ≤ 0.05, **p ≤ 0.01). (E) Relative whole-cell PE levels in wild-type and *yme1Δ* cells treated with DMSO or Rap for 2 h. PE levels are normalized to total lipids. Error bars represent the mean ± SE of four biological replicates. Statistical significance was determined by two-way ANOVA with Holm-Šídák post hoc test comparing each condition to its corresponding DMSO control. (**p ≤ 0.01, ***p ≤ 0.001). (F) Widefield images of wild-type and indicated mutants expressing Tom70-GFP and Tim50-mCherry treated with DMSO or Rap for 2 h. White arrows denote MDCs. Scale bar = 2 μm. (G) Quantification of (F) showing the percentage of cells with MDCs. Error bars represent the mean ± SE of three replicates, *n* ≥ 100 cells per replicate.

Previous work from our laboratory demonstrated that mitochondrial lipid remodeling is important for MDC biogenesis. Specifically, we showed that metabolic stress triggers changes in mitochondrial lipid composition, including a reduction in phosphatidylethanolamine (PE) that is required for MDC formation (Xiao *et al*, 2024). Consistent with this, we previously found that deletion of *UPS2* leads to constitutive MDC formation. How these lipid changes are triggered during MDC induction has remained unclear. The observation that Ups2 accumulates in *yme1Δ* mutants suggested that Yme1 might regulate MDC formation by altering Ups2 abundance. Consistent with this idea, we found that the Rap-induced decline in whole-cell PE previously associated with MDC induction was blunted in *yme1Δ* cells (Fig. 3E). Although the change in PE measured at the whole-cell level is modest, likely due to contributions from non-mitochondrial lipid pools, our previous work demonstrated that similarly small changes in total cellular PE are sufficient to regulate MDC formation (Xiao et al, 2024, Fig. 3E). We next tested whether removal of Ups2 could bypass the requirement for Yme1 in the MDC pathway. In *yme1Δ ups2Δ* double mutants, MDC formation was partially restored. Approximately 14% of untreated double mutant cells formed MDCs, and Rap treatment modestly increased this to ~20% (Fig. 3F–G). Similar trends were observed following treatment with ConcA and CHX, with MDC formation reaching ~24% and ~20%, respectively (Fig. S3A). Notably, MDC formation in the double mutant remained lower than in *ups2Δ* cells alone. These results suggest that while accumulation of Ups2 contributes to the MDC defect in *yme1Δ* cells, removal of Ups2 is not sufficient to fully restore MDC biogenesis in the absence of Yme1. Together, these findings indicate that Yme1 likely promotes MDC formation in part through regulation of mitochondrial lipid transfer pathways and control of PE abundance, but that additional Yme1-regulated factors also contribute to this process.

MICOS complex contributes to Yme1-dependent regulation of MDC formation

The partial rescue of MDC formation in *ups2Δ yme1Δ* mutants suggested that Yme1 regulates the abundance of additional factors that influence MDC biogenesis. Re-examining the proteomics dataset revealed that several components of the MICOS complex—including Mic12, Mic19, Mic26, and Mic27—were significantly elevated in Rap-treated *yme1Δ* cells (Fig. 4A), suggesting that Yme1 may also regulate additional pathways linked to mitochondrial membrane organization, including the MICOS complex, during MDC induction.

The MICOS complex is a conserved multiprotein complex that resides at cristae junctions and maintains the structural organization of the inner mitochondrial membrane (Friedman *et al*, 2015; Huynen *et al*, 2016; Mukherjee *et al*, 2021). In yeast, MICOS consists of six subunits organized into two functional modules: a Mic60–Mic19 subcomplex and a Mic10-containing subcomplex comprising Mic10, Mic12, Mic26, and Mic27 (Friedman *et al*, 2015; Huynen *et al*, 2016;Bohnert *et al*, 2015). Together with ATP synthase dimers, MICOS regulates cristae architecture and also helps maintain connectivity between the inner and outer mitochondrial membranes (Ott *et al*, 2012; Körner *et al*, 2012; Tang *et al*, 2020). Because multiple MICOS components accumulated in *yme1Δ* cells upon Rap treatment, we asked whether disruption of this entire complex influences MDC formation. As the complete MICOS deletion strain lacking all MICOS subunits was generated and characterized previously in the W303 genetic background (Friedman *et al*, 2015), we first verified that MDC formation occurs in this strain background, given that all prior experiments were conducted in the S288C (BY) background. Indeed, Rap treatment induced MDC formation in wild-type W303 cells, although at lower levels (~20%) than typically observed in BY strains (~70%), establishing a lower baseline for this background (Fig. 4B–C). Strikingly, deletion of the MICOS complex resulted in constitutive MDC formation, with ~35% of untreated *MICOSΔ* cells forming MDCs. Rap treatment further increased MDC formation to nearly 50% (Fig. 4B–C). Similar increases were observed following ConcA and CHX treatment (Fig. S3B). These results suggest that disruption of the MICOS complex stimulates MDC biogenesis and that this protein complex normally acts as a constraint on MDC formation.

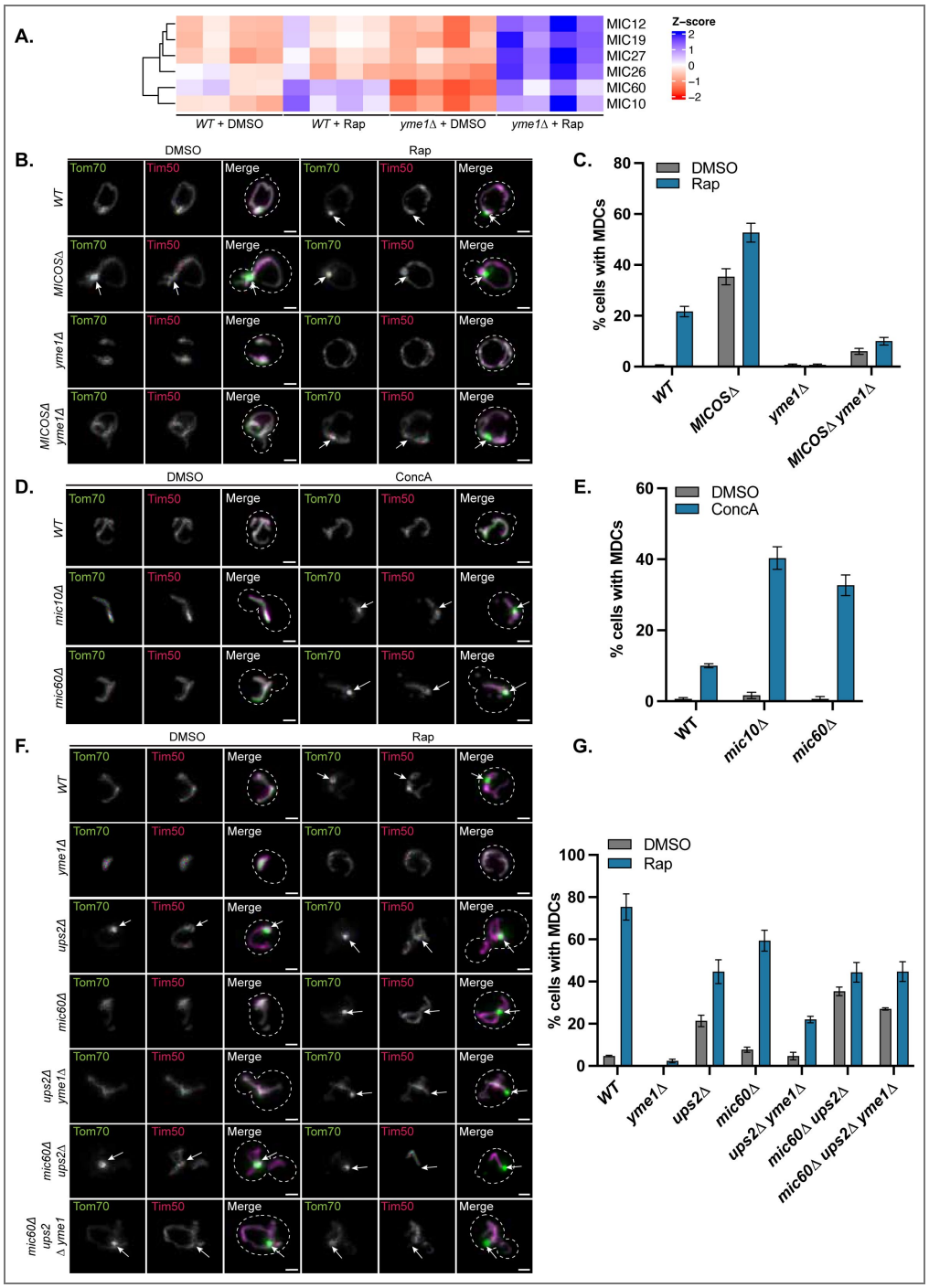

Figure 4. MICOS complex contributes to Yme1-dependent regulation of MDC formation.

(A) Heatmap showing *Z*-scores of MICOS proteins in wild-type and *yme1Δ* cells treated with DMSO or Rap for 2 h (n = 4). Blue indicates upregulated proteins; red indicates downregulated proteins. (B) Widefield images of wild-type and indicated mutants expressing Tom70-GFP and Tim50-mCherry treated with DMSO or Rap for 2 h. White arrows denote MDCs. Scale bar = 2 µm. (C) Quantification of (B) showing the percentage of cells with MDCs. Error bars represent the mean ± SE of three replicates, $n \geq 100$ cells per replicate. (D) Widefield images of wild-type and indicated mutants expressing Tom70-GFP and Tim50-mCherry, grown in media containing low amino acids and treated with DMSO or ConcA for 2 h. White arrows denote MDCs. Scale bar = 2 µm. (E) Quantification of (D) showing the percentage of cells with MDCs. Error bars represent the mean ± SE of three replicates, $n \geq 100$ cells per replicate. (F) Widefield images of wild-type and indicated mutants expressing Tom70-GFP and Tim50-mCherry treated with DMSO or Rap for 2 h. White arrows denote MDCs. Scale bar = 2 µm. (G) Quantification of (F) showing the percentage of cells with MDCs. Error bars represent the mean ± SE of three replicates, $n \geq 100$ cells per replicate.

We next tested whether MICOS deletion could restore MDC formation in *yme1Δ* mutants. While deletion of *YME1* alone blocked MDC formation in W303 cells, MDC formation was partially restored in *MICOSΔ yme1Δ* mutants. Following Rap treatment, approximately 10% of these cells formed MDCs—about half the level observed in wild-type W303 cells (~20%) (Fig. 4B–C). Similar partial restoration was observed following ConcA and CHX treatment (Fig. S3B). These results indicate that altered MICOS abundance contributes to the MDC defect in *yme1Δ* cells but that loss of this complex is not sufficient to fully bypass the requirement for Yme1, similar to the partial bypass effects overserved with loss of Ups2 in strains lacking Yme1.

Combined loss of MICOS components and Ups2 bypasses Yme1 in MDC formation

Because deletion of *UPS2* or disruption of the MICOS complex each partially restored MDC formation in *yme1Δ* cells, we next asked whether combining these perturbations could further bypass the requirement for Yme1. Before testing this interaction, we first tested whether deletion of *UPS2* promotes constitutive MDC formation in the W303 background as it does in the BY background. Indeed, ~30% of untreated ups2Δ W303 cells formed MDCs, with Rap treatment modestly increasing MDC formation to ~40% (Fig. S3C-D). Next, we tested whether simultaneous disruption of MICOS and Ups2 could enhance MDC formation. Indeed, *ups2Δ MICOSΔ* mutants exhibited elevated constitutive MDC formation (~40%), higher than either single mutant, suggesting that lipid transfer (UPS proteins) and mitochondrial architecture (MICOS) represent independent constraints on MDC formation (Fig. S3C-D).

To determine whether loss of both of these pathways could fully bypass Yme1, we attempted to construct a *MICOSΔ ups2Δ yme1Δ* triple mutant. However, this strain was not viable, preventing direct analysis of complete MICOS disruption in this context. To overcome this limitation, we examined individual MICOS subunits to identify components with the strongest influence on MDC formation. Deletion strains were generated in the BY background and tested for MDC formation. Unlike the full MICOS deletion, under nutrient-rich conditions, deletion of individual MICOS subunits did not constitutively activate MDC formation nor did it significantly alter MDC formation upon ConcA, Rap, or CHX treatment compared to wild-type cells (Fig. S3E). However, when MDC formation was examined under metabolically restrictive conditions (low amino acid media), which normally block ConcA-induced MDC formation, deletion of specific MICOS components restored MDC formation. Under these conditions, *mic10Δ* mutants displayed MDC formation in ~40% of ConcA-treated cells and mic60Δ mutants in ~30%, compared to ~10% in wild-type (Fig. 4D–E). Deletion of additional MICOS subunits (mic27Δ, mic12Δ, and mic19Δ) also increased MDC formation to a lesser extent, while mic26Δ had little effect (Fig. S4A–B), indicating that loss of MICOS components variably sensitizes cells to MDC formation.

Based on these results, we generated triple-mutant strains combining *ups2Δ* and *yme1Δ* with deletion of either *MIC10* or *MIC60*. The *mic60Δ ups2Δ yme1Δ* strain showed substantially restored MDC formation, with ~27% of untreated cells forming MDCs and ~45% forming MDCs following Rap treatment (Fig. 4F-G). These results indicate that simultaneous disruption of Ups2 and Mic60 can largely bypass the requirement for Yme1. Notably, a *mic60Δ yme1Δ* double mutant could not be generated due to synthetic lethality in the BY background, highlighting a strong functional interaction between these pathways (Fig. S4C). The *mic10Δ ups2Δ yme1Δ* strain exhibited partial rescue of basal MDC formation (~24%) but did not respond strongly to MDC inducers (Fig. S4D-E). Together, these findings indicate that multiple mitochondrial constraints—including lipid composition and MICOS—must be altered to permit MDC formation, and that Yme1 promotes MDC biogenesis by coordinately regulating these pathways.

Yme1-dependent MDC formation is gated by metabolic cues

Having established that Yme1 controls MDC formation by regulating lipid transfer proteins and MICOS, we next asked how this activity is controlled and whether increasing Yme1 levels is sufficient to drive MDC biogenesis. As shown in Figure 1G–H, overexpression of Yme1 triggered MDC formation in a large fraction of untreated cells, and this effect required Yme1 proteolytic

activity, as a catalytically inactive mutant failed to induce MDCs. Importantly, several of the Yme1-regulated factors identified in our proteomic analysis—including Ups proteins and MICOS components—are altered in abundance even at steady state in the absence of Yme1 and become further altered during MDC-inducing conditions such as Rap treatment. These observations suggest that Yme1-dependent regulation of mitochondrial proteins occurs constitutively, but is amplified during stress, resulting in greater remodeling of lipid transfer pathways and MICOS. Consistent with this idea, Yme1 overexpression-driven MDC formation remained dependent on metabolic context. In contrast to overexpressing Yme1 in nutrient rich medium (Fig. 1G-H), overexpressing Yme1 in minimal media lacking amino acids did not stimulate MDC formation (Fig. 5A–B). Thus, even when Yme1 levels are elevated, MDC biogenesis requires a permissive metabolic environment.

Together with the genetic and proteomic observations described above, these findings support a model in which Yme1 promotes MDC biogenesis by progressively relieving lipid and membrane organizational constraints imposed by the Ups pathway and MICOS. Under basal conditions, Yme1 activity likely contributes to ongoing mitochondrial remodeling but is insufficient to trigger widespread MDC formation. During metabolic stress, however, this remodeling is amplified—either through increased Yme1 activity or through changes in substrate susceptibility that enhance Yme1-dependent turnover—thereby permitting MDC biogenesis. The inability of Yme1 overexpression to induce MDCs under restrictive metabolic conditions further indicates that additional metabolic inputs gate pathway activation. This model, summarized below and provided Figure 5C, places Yme1 as a central regulator that removes constraints on MDC formation, while metabolic signals determine when this remodeling is sufficient to drive the pathway.

Summary and model for Yme1-dependent regulation of mitochondrial-derived compartment biogenesis

Mitochondrial membranes dynamically remodel in response to metabolic shifts and cellular stress. In previous work, we identified the mitochondrial-derived compartment (MDC) pathway as a mechanism of outer mitochondrial membrane remodeling that selectively sequesters hydrophobic OMM proteins during metabolic and proteotoxic stress. MDC formation was previously shown to depend on metabolic signals that alter mitochondrial lipid composition, particularly reductions in phosphatidylethanolamine (PE). However, the molecular mechanisms that translate these metabolic signals into the membrane remodeling events required for MDC formation have remained unclear.

In this study, we identify the conserved mitochondrial i-AAA protease Yme1 as a central regulator of MDC biogenesis. Through genetic, proteomic, and biochemical approaches, we find that Yme1 promotes MDC formation by remodeling multiple mitochondrial pathways that normally act as constraints on OMM remodeling. Our data implicate the Ups lipid transfer pathway and the MICOS complex, two systems that regulate mitochondrial lipid homeostasis and membrane organization. Disruption of either pathway partially restores MDC formation in *yme1Δ* cells, whereas combined perturbation of both pathways largely bypasses the requirement for Yme1. These findings imply that MDC formation may require coordinated remodeling of both mitochondrial lipid composition and mitochondrial membrane organization.

How these pathways constrain MDC formation remains an important open question. One possibility is that Yme1-mediated turnover of Ups proteins alters mitochondrial lipid composition and/or redistributes lipids between the IMM and OMM, including local PE levels, thereby promoting membrane curvature or generating OMM membrane domains permissive for MDC formation (Agrawal & Ramachandran, 2019; Xiao *et al*, 2024). Interestingly, studies in mammalian systems have shown that the Yme1 ortholog YME1L is itself regulated by mitochondrial lipid composition (MacVicar *et al*, 2019), including PE levels, suggesting that lipid homeostasis and Yme1-family proteases may participate in conserved feedback mechanisms that couple mitochondrial membrane composition to protease activity. In parallel, the MICOS complex organizes crista junctions and maintains associations between the IMM and OMM (Körner *et al*, 2012; Ott *et al*, 2012; Zerbes *et al*, 2012; Aaltonen *et al*, 2016; Cogliati *et al*, 2016). Loss

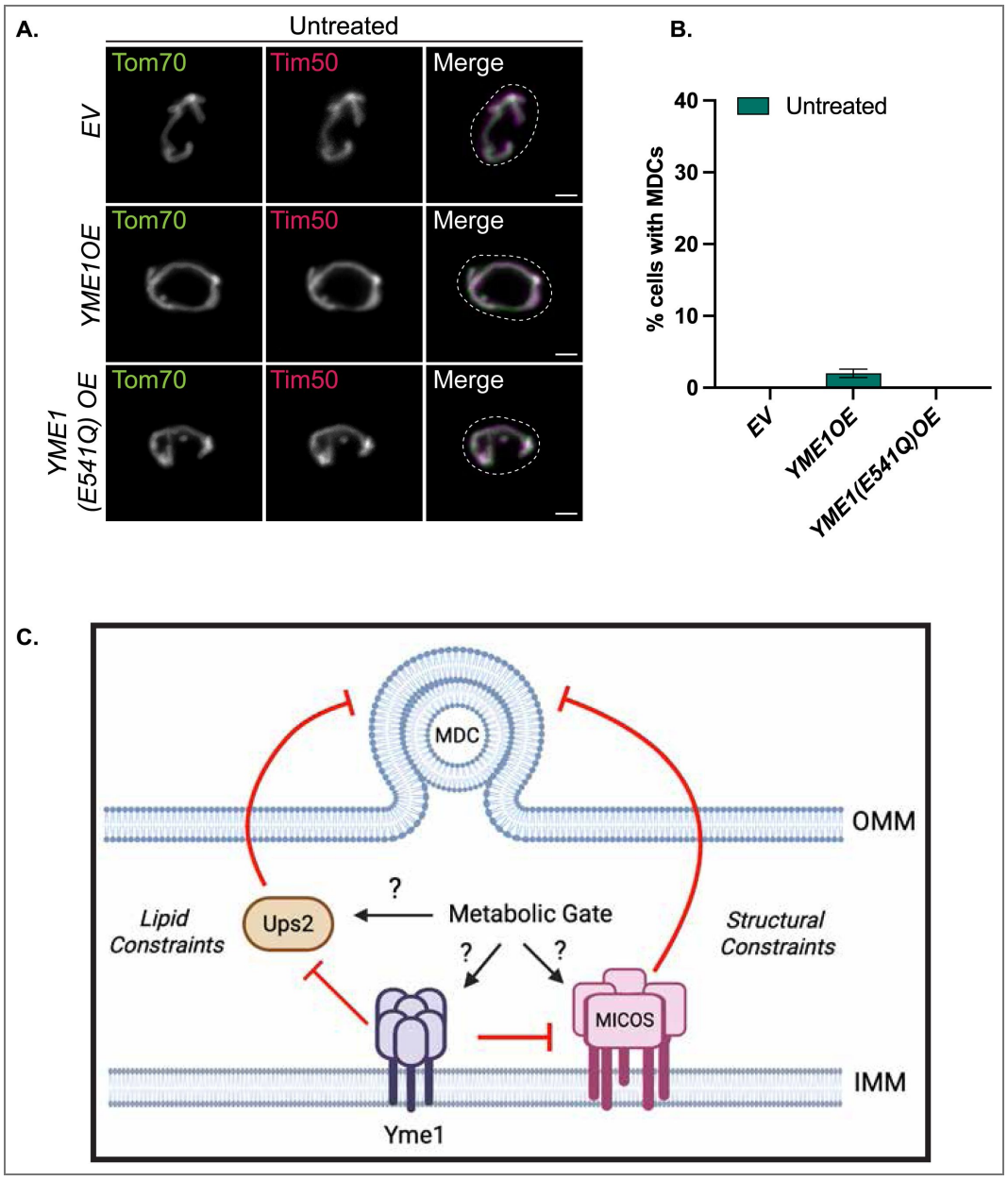

Figure 5. Yme1-dependent MDC formation is gated by metabolic cues.

(A) Widefield images of yeast cells tagged with Tom70-GFP and Tim50-mCherry, constitutively overexpressing *YME1* (*YME1 OE*), the protease-dead mutant, *YME1(E541Q)*, or an empty vector (*EV*) control grown in minimal media that lacks amino acids. Scale bar = 2 μm. (B) Quantification of (A) showing the percentage of cells with MDCs. Error bars represent the mean ± SE of three replicates, $n \geq 100$ cells per replicate. (C) Model of Yme1-mediated MDC biogenesis: Upon treatment with MDC stimulating stressors, Yme1 degrades Ups2, altering lipids, while also modulating the MICOS complex to possibly alter organizational or structural constraints that normally inhibit MDC formation. Panel C created with *BioRender.com*.

of MICOS may therefore disrupt membrane associations or alter lipid distribution between mitochondrial subcompartments, indirectly promoting OMM remodeling into MDCs. In this framework, Yme1-dependent remodeling of lipid transfer pathways and mitochondrial membrane organization relieves constraints that would otherwise limit the formation of MDCs. Notably, additional Yme1-sensitive proteins were altered in the proteomics dataset, including IMS-localized components of mitochondrial protein import, suggesting that the partly incomplete bypass of Yme1 by combining *ups2Δ* and *MICOSΔ* may reflect contributions from additional downstream effectors.

Our findings further indicate that Yme1-dependent remodeling occurs constitutively but is somehow responsive to metabolic stress. Several Yme1-regulated proteins change in abundance even under steady-state conditions and undergo further remodeling following MDC-inducing treatments such as rapamycin. Consistent with this idea, increasing Yme1 levels through overexpression is sufficient to induce MDC formation in otherwise untreated cells. However, this effect remains dependent on metabolic context, as Yme1 overexpression does not stimulate MDCS when cells are shifted to amino-acid-free media. These observations suggest that metabolic signals gate MDC formation by modulating either Yme1 activity itself or its substrates, or other downstream steps required for compartment formation.

Based on these observations, we propose the model summarized in Figure 5C. In this model, Yme1 acts as a central regulator that promotes MDC formation by progressively removing lipid and organizational constraints that normally stabilize mitochondrial membranes. Under basal conditions, Yme1-mediated turnover of key substrates contributes to ongoing mitochondrial remodeling but is insufficient to trigger widespread MDC formation. During metabolic stress, however, this remodeling is amplified—either through increased Yme1 activity or alterations in its substrates—allowing MDC biogenesis to proceed. In this way, MDC formation emerges as the outcome of coordinated changes in mitochondrial lipid composition, membrane organization, and metabolic state. Together, these findings position Yme1 as a key integrator of mitochondrial proteostasis, membrane organization, and metabolic signaling in the control of MDC formation.

Materials and methods

Yeast strains

Saccharomyces cerevisiae strains used in this study are described in Table S1 and are derivatives of either S288C (Brachmann *et al*, 1998) or W303 (Matheson *et al*, 2017). All deletion mutants described in this study were generated via sporulation. In a diploid, one allele of the target gene was deleted by PCR mediated gene replacement using the previously described pRS series of vectors (Sikorski & Hieter; Andersen, 2012) and oligo pairs listed in Table S2. Insertion of the selection cassette was verified by colony PCR across the chromosomal integration site. The confirmed heterozygous diploids gene deletions were subsequently sporulated to generate haploid mutants. Strains expressing fluorescently tagged proteins were created by PCR-mediated C-terminal endogenous epitope tagging using standard techniques and oligo pairs listed in Table S2. Plasmid templates for fluorescent epitope tagging were from the pKT series of vectors (Sheff & Thorn, 2004). Correct integrations were confirmed by correctly localized expression of the fluorophore by microscopy. Further, HA-tagged strains were generated by PCR-mediated C-terminal endogenous tagging using pFA6A-3xHA-KanMX (Bähler *et al*, 1998) as the template plasmid and oligonucleotides listed in Table S2, with correct integration confirmed by colony PCR and western blotting. Yeast strains AHY 15346, AHY 15348, and AHY15438 were rendered prototrophic with pHLUM (Mülleder *et al*, 2012) to eliminate complications arising from amino acid auxotrophies and were subsequently used to assess amino acid dependencies on MDC formation.

Plasmids

Plasmids used in this study are listed in Table S3. pHLUM, a yeast plasmid expressing multiple auxotrophic marker genes from their endogenous promoters, was obtained from Addgene (# 40276) (Mülleder *et al*, 2012). Plasmids for GPD driven expression of *YME1* were generated by Gateway mediated transfer of corresponding ORF (Harvard Institute of Proteomics) from pDONR221 into a pAG306-ccdB chromosome I (Hughes & Gottschling, 2012) using Gateway LR Clonase II enzyme mix (ThermoFisher) according to the manufacturer's instructions. All insert sequences were verified by Azenta/Genewiz sequencing. The resulting expression plasmid was digested with NotI and integrated into yeast chromosome I (199456-199457).

Cell culture and media

Yeast cells were grown exponentially for 15–16 h at 30°C (OD_{600}= 0.2–0.8) before the start of all experiments. This period of overnight log-phase growth is required to ensure mitochondrial uniformity across the cell population and is critical for MDC biogenesis. Unless indicated, cells were cultured in YPAD medium (1% yeast extract, 2% peptone, 0.005% adenine, 2% glucose). For amino acid dependency experiments, SD medium (low amino acid medium) (0.67% yeast nitrogen base without amino acids, 2% glucose, supplemented with the following nutrients 0.074 g/liter each of adenine, alanine, arginine, asparagine, aspartic acid, cysteine, glutamic acid, glutamine, glycine, histidine, myoinositol, isoleucine, lysine, methionine, phenylalanine, proline, serine, threonine, tryptophan, tyrosine, uracil, valine, 0.369 g/liter of leucine, 0.007 g/liter of para-aminobenzoic acid) or minimal medium i.e. no amino acid medium (0.67% yeast nitrogen base without amino acids, 2% glucose) was used. Where indicated, cells were treated with rapamycin, concanamycin A, or cycloheximide at final concentrations of 200nM, 500nM, or 10ug/mL respectively to induce MDC biogenesis.

MDC assays

For MDC assays, overnight log-phase cultures were either directly harvested or after a two-hour treatment with dimethyl sulfoxide (DMSO) or the indicated drug. For MDC assays with plasmid-containing cells, overnight log-phase yeast cultures were grown in selective SD medium, back-diluted to an OD_{600} of 0.2–0.4 in YPAD, and treated with DMSO or the indicated MDC inducer for 2 h. Prior to visualization, cells were harvested by centrifugation, washed once with distilled water, resuspended in an imaging buffer (5% wt/vol Glucose, 10 mM HEPES, pH 7.6) and imaged as described below.

Microscopy and image analysis

Yeast were plated onto a slide at small volumes to allow for the formation of a monolayer. Optical z-sections of live yeast cells were acquired with a Zeiss Axiocam 506 monochromatic camera and 63 x oil immersion objectives (Carl Zeiss, Plan Apochromat, NA 1.4). To obtain super-resolution images a ZEISS LSM800 confocal microscope equipped with an Airyscan detector and 63 x oil immersion objective (Carl Zeiss, Plan Apochromat, NA 1.4) was used. Maximum intensity projected widefield images generated in Zen (Carl Zeiss) were used to quantify the percentage of cells with MDCs. MDCs were identified as Tom70-positive, Tim50-negative structures that were enriched for Tom70 versus the mitochondrial tubule. Unless indicated, maximum-intensity projected images are displayed for all images. All MDC quantifications show the mean ± SE from at least three biological replicates with n≥100 cells per experiment. Representative images were processed using Fiji. Maximum intensity projections of individual channels were generated, and fluorescence intensities were minimally adjusted for visualization to enable comparison across channels. Line-scan analyses were performed on non-adjusted single z-sections.

Protein preparation and immunoblotting

Yeast cultures were grown overnight as described and treated with either DMSO or Rap. Post treatment, 2 OD_{600} units of cells were collected, washed twice with distilled water and incubated in 0.1M NaOH for 5 min at RT. The pellet was reisolated at 14,000 × g for 10 min at 4°C and resuspended in lysis buffer (10 mM Tris, pH 6.8; 100 mM NaCl; 1 mM EDTA; 1 mM EGTA; 1% SDS; cOmplete™ protease inhibitor cocktail, Millipore Sigma) for 5 min at 95°C. Subsequently, samples were denatured in Laemmli buffer (63 mM Tris pH 6.8, 2% SDS, 10% glycerol, 1 mg/ml bromophenol blue, 1% β-mercaptoethanol) for 5 min at 95°C. The prepared protein samples were resolved on a 4–12% SDS–polyacrylamide gradient gel and transferred onto nitrocellulose membranes using a semi-dry transfer system. To prevent nonspecific antibody binding, membranes were blocked in Tris-buffered saline with 0.05% Tween-20 (TBST) containing 10% nonfat dry milk for 40 min at RT, followed by overnight incubation with indicated primary antibodies at 4°C. Membranes were washed four times with TBST and incubated with secondary antibody (donkey anti-mouse HRP-conjugated, 1:4000 in TBST containing 10% nonfat dry milk; Sigma-Aldrich) for 1 h at room temperature. Following incubation, membranes were washed twice with TBST and twice with TBS. Blots were developed using enhanced chemiluminescence substrate (Thermo Fisher Scientific), and signals were detected with a Bio-Rad ChemiDoc MP system. Images were exported as TIFF files and cropped in Adobe Illustrator.

Analysis of protein levels using FIJI

Raw TIFF images were imported into FIJI for densitometric analysis. A standardized rectangular region of interest was applied to each band to obtain the integrated density (AU). To correct for background, four measurements were taken from blank regions of each blot and averaged. Each band intensity was normalized first to its respective loading control within the same lane and then to the corresponding wild-type untreated sample. Quantification was performed using three independent replicates per condition. Data were plotted in GraphPad Prism, and p-values were calculated using two-way ANOVA.

Quantification and statistical analysis

No randomization or blinding was performed, as all experiments were conducted using defined laboratory reagents and yeast strains with known genotypes. For all experiments, biological replicates are represented by “n,” with at least three replicates per experiment. All statistical analyses were conducted in GraphPad Prism, with the specific tests and measures of dispersion and precision reported in the figure legends.

Mitochondrial proteomics Isolation of yeast mitochondria

Yeast were grown overnight to log-phase (OD_{600}= 0.4–0.8) and treated with either DMSO or Rap for 2 h. Subsequently, cells were isolated by centrifugation, washed with distilled water, and the pellet weight was recorded. The pellets were resuspended in dithiothreitol (DTT) buffer (0.1 M Tris, 10 mM DTT, pH 9.4) at 2mL per gram of the pellet and incubated for 20 min at 30°C under constant rotation. After reisolation by centrifugation, DTT treated cells were washed once in 1.2M sorbitol and resuspended in sorbitol phosphate buffer (6.7 mL per gram of pellet) containing 2 mg of lyticase per gram of pellet. Cells were incubated for 30–45 min at 30°C with constant rotation to digest the cell wall and generate spheroplasts. Following lyticase treatment, spheroplasts were isolated by centrifugation and lysed by mechanical disruption in homogenization buffer (0.6 M sorbitol, 10 mM Tris, pH 7.4, 1 mM EDTA, pH 8.0 adjusted with KOH, 0.2% BSA, 1 mM PMSF) at 13.3 mL per gram of pellet at 4°C. Cell debris was removed from the homogenate twice by centrifugation at 2,000 × g for 5 min each at 4°C and mitochondria were pelleted at 17,500 × g for 12 min at 4°C. The mitochondrial pellet was resuspended in SEM buffer (250 mM sucrose, 1 mM EDTA, pH 8.0 adjusted with KOH, 10 mM 3-(N-morpholino)-prop-ansulfonic acid, pH 7.2), and reisolated by differential centrifugation as described above, and subsequently resuspended in

SEM buffer. The protein concentration of mitochondria was determined by Bicinchoninic Acid (BCA) Assay. For proteomics analysis, 100 µg of mitochondria (by protein) were pelleted, shock-frozen in liquid nitrogen, and stored at −80°C.

Mass spectrometry sample preparation

Samples for protein analysis were prepared essentially as previously described (Navarrete-Perea *et al*, 2018; Li *et al*, 2021). Proteomes were extracted using a buffer containing 200 mM EPPS pH 8.5, 8M urea, 0.1% SDS and protease inhibitors. Following lysis, 25 µg of each proteome was reduced with 5 mM TCEP. Cysteine residues were alkylated using 10 mM iodoacetimide for 20 minutes at RT in the dark. Excess iodoacetimide was quenched with 10 mM DTT. A buffer exchange was carried out using a modified SP3 protocol (Hughes *et al*, 2019). Briefly, ~250 µg of Cytiva SpeedBead Magnetic Carboxylate Modified Particles (65152105050250 and 4515210505250), mixed at a 1:1 ratio, were added to each sample. 100% ethanol was added to each sample to achieve a final ethanol concentration of at least 50%. Samples were incubated with gentle shaking for 15 minutes. Samples were washed three times with 80% ethanol. Protein was eluted from SP3 beads using 200 mM EPPS pH 8.5 containing Lys-C (Wako, 129-02541). Samples were digested overnight at room temperature with vigorous shaking. The next morning trypsin was added to each sample and further incubated for 6 hours at 37° C. Acetonitrile was added to each sample to achieve a final concentration of ~33%. Each sample was labelled, in the presence of SP3 beads, with ~62.5 µg of TMTPro reagents (ThermoFisher Scientific). Following confirmation of satisfactory labelling (>97%), excess TMT was quenched by addition of hydroxylamine to a final concentration of 0.3%. The full volume from each sample was pooled and acetonitrile was removed by vacuum centrifugation for 1 hour. The pooled sample was acidified and peptides were de-salted using a Sep-Pak 50mg tC18 cartridge (Waters). Peptides were eluted in 70% acetonitrile, 1% formic acid and dried by vacuum centrifugation.

Basic pH reversed-phase separation (BPRP)

TMT labeled peptides were solubilized in 5% acetonitrile/10 mM ammonium bicarbonate, pH 8.0 and ~300 µg of TMT labeled peptides were separated by an Agilent 300 Extend C18 column (3.5 mm particles, 4.6 mm ID and 250 mm in length). An Agilent 1260 binary pump coupled with a photodiode array (PDA) detector (Thermo Scientific) was used to separate the peptides. A 45 minute linear gradient from 10% to 40% acetonitrile in 10 mM ammonium bicarbonate pH 8.0 (flow rate of 0.6 mL/min) separated the peptide mixtures into a total of 96 fractions (36 seconds). A total of 96 Fractions were consolidated into 24 samples in a checkerboard fashion and vacuum dried to completion. Each sample was desalted via Stage Tips and re-dissolved in 5% formic acid/5% acetonitrile for LC-MS3 analysis.

Liquid chromatography and tandem mass spectrometry

Mass spectrometric data were collected on an Orbitrap Eclipse mass spectrometer coupled to a Proxeon NanoLC-1000 UHPLC (Thermo Fisher Scientific). The 100 µm capillary column was packed in-house with 35 cm of Accucore 150 resin (2.6 µm, 150Å; ThermoFisher Scientific). Data were acquired for 120 min per run. A FAIMS device was enabled during data collection and compensation voltages were set at -40V, -60V, and -80V (Schweppe *et al*, 2019). MS1 scans were collected in the Orbitrap (resolution – 60,000; scan range – 400-1600 Th; automatic gain control (AGC) – $4x10^5$, maximum ion injection time – automatic). MS2 scans were collected in the Orbitrap following higher-energy collision dissociation (HCD; resolution – 50,000; AGC – $1.25x10^5$; normalized collision energy – 36; isolation window – 0.5 Th; maximum ion injection time – 86 ms.

Mass spectrometry data analysis

Database searching included all entries from the Saccharomyces cerevisiae UniProt Database (downloaded in June 2023). The database was concatenated with one composed of all protein sequences for that database in the reversed order (Elias JE *et al*, 2007). Raw files were converted to mzXML, and monoisotopic peaks were re-assigned using Monocle (Rad *et al*, 2021). Searches

were performed with Comet (Eng *et al*, 2013) using a 50-ppm precursor ion tolerance and fragment bin tolerance of 0.02. TMTpro labels on lysine residues and peptide N-termini (+304.207 Da), as well as carbamidomethylation of cysteine residues (+57.021 Da) were set as static modifications, while oxidation of methionine residues (+15.995 Da) was set as a variable modification. Peptide-spectrum matches (PSMs) were adjusted to a 1% false discovery rate (FDR) using a linear discriminant after which proteins were assembled further to a final protein-level FDR of 1% analysis (Huttlin *et al*, 2010). TMT reporter ion intensities were measured using a 0.003 Da window around the theoretical m/z for each reporter ion. Proteins were quantified by summing reporter ion counts across all matching PSMs. More specifically, reporter ion intensities were adjusted to correct for the isotopic impurities of the different TMTpro reagents according to manufacturer specifications. Peptides were filtered to exclude those with a summed signal-to-noise (SN) < 180 across all TMT channels and < 0.5 precursor isolation specificity. The signal-to-noise (S/N) measurements of peptides assigned to each protein were summed (for a given protein). The mass spectrometry proteomics data have been deposited to the ProteomeXchange Consortium via the PRIDE (Perez-Riverol *et al*, 2025) partner repository with the dataset identifier PXD075997. Table S4 provides a summary of peptide counts and signal-to-noise (S/N) ratios across all identified proteins in all samples.

Statistical analysis and data visualization

Proteomics data were $\log_2$-transformed prior to analysis. Principal component analysis (PCA) was performed using the NIPALS algorithm (Wright K, 2025) to evaluate sample clustering. Boxplots with color and pattern fills were used to compare protein expression across treatment and genotype groups, respectively. Differences in protein abundance between groups were assessed using Welch's two-sample t-tests. Proteins were considered differentially expressed if they exhibited at least a 1.5-fold change in either direction and Storey's q-value ≤ 0.05 (Storey & Tibshirani, 2003). Volcano plots were generated to visualize fold changes and significance. Z-score normalized values of selected proteins were visualized in heatmaps with hierarchical clustering using the ComplexHeatmap R package (Gu *et al*, 2016; Gu, 2022). Protein annotations were retrieved from UniProt (The UniProt Consortium *et al*, 2025) on 2025-02-12 to obtain Gene Ontology (GO) terms. Table S5 details the Gene Ontology (GO) annotations associated with the proteins identified in Table S4. Pathway enrichment analysis was performed using the gprofiler2 (Kolberg *et al*, 2020) R package (organism = "scerevisiae"), which queries multiple databases by default. For visualization and interpretation, enrichment results were filtered to the GO:Biological Process (GO:BP) category. Table S6 summarizes the corresponding functional enrichment results generated using g:Profiler.

Whole-cell lipidomics sample preparation

Yeast cells were grown overnight as described above and treated with the indicated inducers. Following treatment, 5 OD_{600} units of cells were harvested, washed twice with dH_2O, and flash-frozen. Extraction of lipids was carried out using a biphasic solvent system of cold methanol, methyl *tert*-butyl ether (MTBE), and PBS (Matyash *et al*, 2008) with some modifications. In a randomized sequence, to each sample was added 230 µL MeOH with internal standards. Samples were homogenized for 30 seconds, transferred to microcentrifuge tubes (polypropylene 1.7 mL, VWR, USA) containing 750 µL MTBE, and then incubated on ice with occasional vortexing for 1 hr. Following incubation, samples were centrifuged at 15,000 x g for 10 minutes at 4°C. The organic (upper) layer was collected, and the aqueous (lower) layer was re-extracted with 1 mL of 10:3:2.5 (*v/v/v*) MTBE/MeOH/dd-H2O, briefly vortexed, incubated at RT, and centrifuged at 15,000 x g for 10 minutes at 4°C. Upper phases were combined and evaporated to dryness under speedvac. Lipid extracts were reconstituted in 250 µL of 4:1:1 (v/v/v) IPA/ACN/water and transferred to LC-MS vials for analysis. Concurrently, a process blank sample was prepared and pooled quality control (QC) samples were prepared by taking equal volumes from each sample after final resuspension.

LC-MS analysis (QTOF)

Lipid extracts were separated on an Acquity UPLC CSH C18 column (2.1 x 100 mm; 1.7 µm) coupled to an Acquity UPLC CSH C18 VanGuard precolumn (5 × 2.1 mm; 1.7 µm) (Waters, Milford, MA) maintained at 65°C connected to an Agilent HiP 1290 Sampler, Agilent 1290 Infinity pump, and Agilent 6545 Accurate Mass Q-TOF dual AJS-ESI mass spectrometer (Agilent Technologies, Santa Clara, CA). Samples were analyzed in a randomized order in both positive and negative ionization modes in separate experiments acquired with the scan range m/z 100 – 1700. For positive mode, the source gas temperature was set to 225°C, with a drying gas flow of 11 L/min, nebulizer pressure of 40 psig, sheath gas temp of 350°C and sheath gas flow of 11 L/min. VCap voltage is set at 3500 V, nozzle voltage 500V, fragmentor at 110 V, skimmer at 85 V and octopole RF peak at 750 V. For negative mode, the source gas temperature was set to 300°C, with a drying gas flow of 11 L/min, a nebulizer pressure of 30 psig, sheath gas temp of 350°C and sheath gas flow 11 L/min. VCap voltage was set at 3500 V, nozzle voltage 75 V, fragmentor at 175 V, skimmer at 75 V and octopole RF peak at 750 V. Mobile phase A consisted of ACN:H_2O (60:40, *v/v*) in 10 mM ammonium formate and 0.1% formic acid, and mobile phase B consisted of IPA:ACN:H_2O (90:9:1, *v/v/v*) in 10 mM ammonium formate and 0.1% formic acid. For negative mode analysis the modifiers were changed to 10 mM ammonium acetate. The chromatography gradient for both positive and negative modes started at 15% mobile phase B then increased to 30% B over 2.4 min, it then increased to 48% B from 2.4 – 3.0 min, then increased to 82% B from 3 – 13.2 min, then increased to 99% B from 13.2 – 13.8 min where it's held until 16.7 min and then returned to the initial conditions and equilibrated for 5 min. Flow was 0.4 mL/min throughout, with injection volumes of 1 µL for positive and 10 µL negative mode.

Tandem mass spectrometry was conducted using iterative exclusion, the same LC gradient at collision energies of 20 V and 27.5 V in positive and negative modes, respectively.

LC-MS data processing

For data processing, Agilent MassHunter (MH) Workstation and software packages MH Qualitative and MH Quantitative were used. The pooled QC (n=8) and process blank (n=4) were injected throughout the sample queue to ensure the reliability of acquired lipidomics data. For lipid annotation, accurate mass and MS/MS matching was used with the Agilent Lipid Annotator library and LipidMatch (Koelmel *et al*, 2017). Results from the positive and negative ionization modes from Lipid Annotator were merged based on the class of lipid identified. Data exported from MH Quantitative was evaluated using Excel where initial lipid targets are parsed based on the following criteria. Only lipids with relative standard deviations (RSD) less than 30% in QC samples are used for data analysis. Additionally, only lipids with background AUC counts in process blanks that are less than 30% of QC are used for data analysis. The parsed excel data tables are normalized based on the ratio to class-specific internal standards, then to tissue mass and sum prior to statistical analysis.

Statistical analysis and data visualization

Four biological replicates were used for each lipidomics experiment and analyzed within the same LC-MS run. Statistical analysis was performed in GraphPad Prism using two-way ANOVA with Holm–Sidak post hoc tests, as indicated in the figure legends. All data were included except those that did not meet QC criteria; if a replicate failed QC, the entire biological replicate was excluded from further analysis. For each denoted phospholipid, all corresponding lipid species were considered, and values were normalized to OD of whole-cell lysates. Table S7 summarizes cumulative lipid levels across samples, including PE abundance and the corresponding percentage of PE relative to total lipid content.

Supplemental material

Figure S1 shows that secondary effects related to loss of Yme1 do not impact MDC formation. Figure S2 depicts quality control analyses of the TMT-based mitoproteomics dataset including data normalization (box plots) and principal component analysis (PCA). Figure S3 shows MDC assay profiling of Yme1-regulated factors in the MDC pathway. Figure S4 highlights the role of the MICOS complex in MDC biogenesis, including the effects of individual MICOS mutants and their genetic interactions with Yme1 and Ups2. Table S1 lists the yeast strains used in this study. Table S2 contains the oligonucleotides used in this study. Table S3 includes bacterial strains, chemicals, antibodies, plasmids, and software used in this study. Table S4 contains the TMT-based quantitative proteomics dataset, containing the peptide counts and scaled signal-to-noise (S/N) values for all identified proteins across all samples. Table S5 lists the Gene Ontology (GO) annotations associated with the identified proteins listed in Table S4. Table S6 contains the functional enrichment analysis performed using g:Profiler. Table S7 summarizes total lipid levels, including the relative and/or absolute abundance of PE levels measured across the indicated conditions.

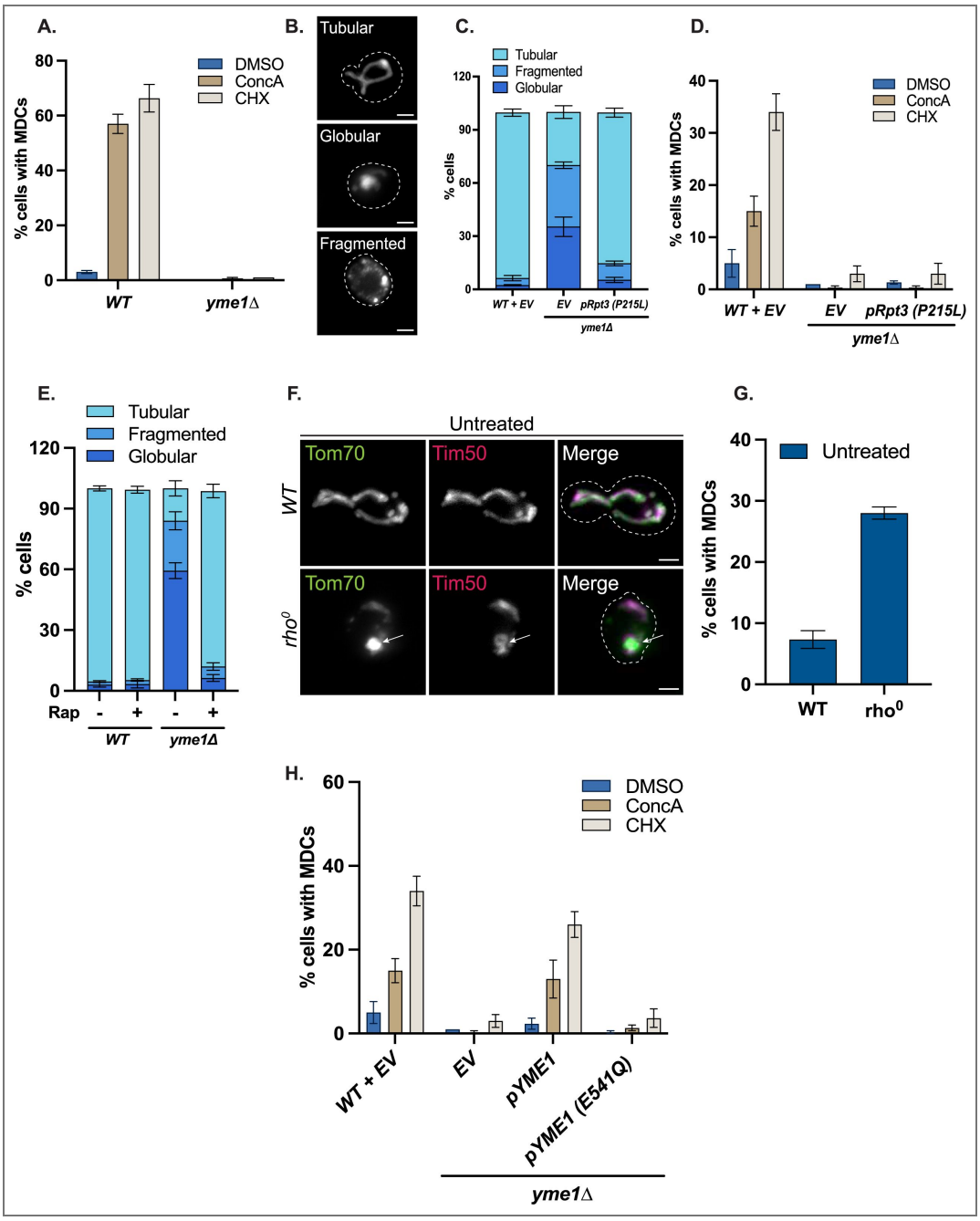

Figure S1. Secondary effects related to loss of Yme1 do not impact MDC formation (Related to Figure 1).

(A) Quantification of MDC formation in wild-type and *yme1Δ* cells treated with DMSO, ConcA, or CHX for 2 h. Error bars represent the mean ± SE of three replicates, *n* ≥ 100 cells per replicate. (B) Representative widefield images of distinct yeast mitochondrial morphologies. Scale bar = 2 µm. (C) Quantification of mitochondrial morphology in wild-type and *yme1Δ* cells expressing either *EV* or *pRS413-Rpt3 (P215L)*. Error bars represent the mean ± SE of three replicates, *n* ≥ 100 cells per replicate. (D) Quantification of MDC formation in wild-type and *yme1Δ* cells expressing either *EV* or *pRS413-Rpt3 (P215L)* treated with DMSO, ConcA, or CHX for 2 h. Error bars represent the mean ± SE of three replicates, *n* ≥ 100 cells per replicate. (E) Quantification of mitochondrial morphology in wild-type and *yme1Δ* cells treated with DMSO or Rap for 2 h. Error bars represent the mean ± SE of three replicates, *n* ≥ 100 cells per replicate. (F) Widefield images of wild-type and *rho*^{0} cells expressing Tom70-GFP and Tim50-mCherry. White arrows denote MDCs. White arrows denote MDCs. Scale bar = 2 µm. (G) Quantification of (F) showing the percentage of cells with MDCs. Error bars represent the mean ± SE of three replicates, *n* ≥ 100 cells per replicate. (H) Quantification of MDC formation in wild-type and *yme1Δ* cells expressing either *EV*, pRS413-Yme1, or pRS413-Yme1 (E541Q) treated with DMSO, ConcA, or CHX for 2 h. Error bars represent the mean ± SE of three replicates, *n* ≥ 100 cells per replicate.

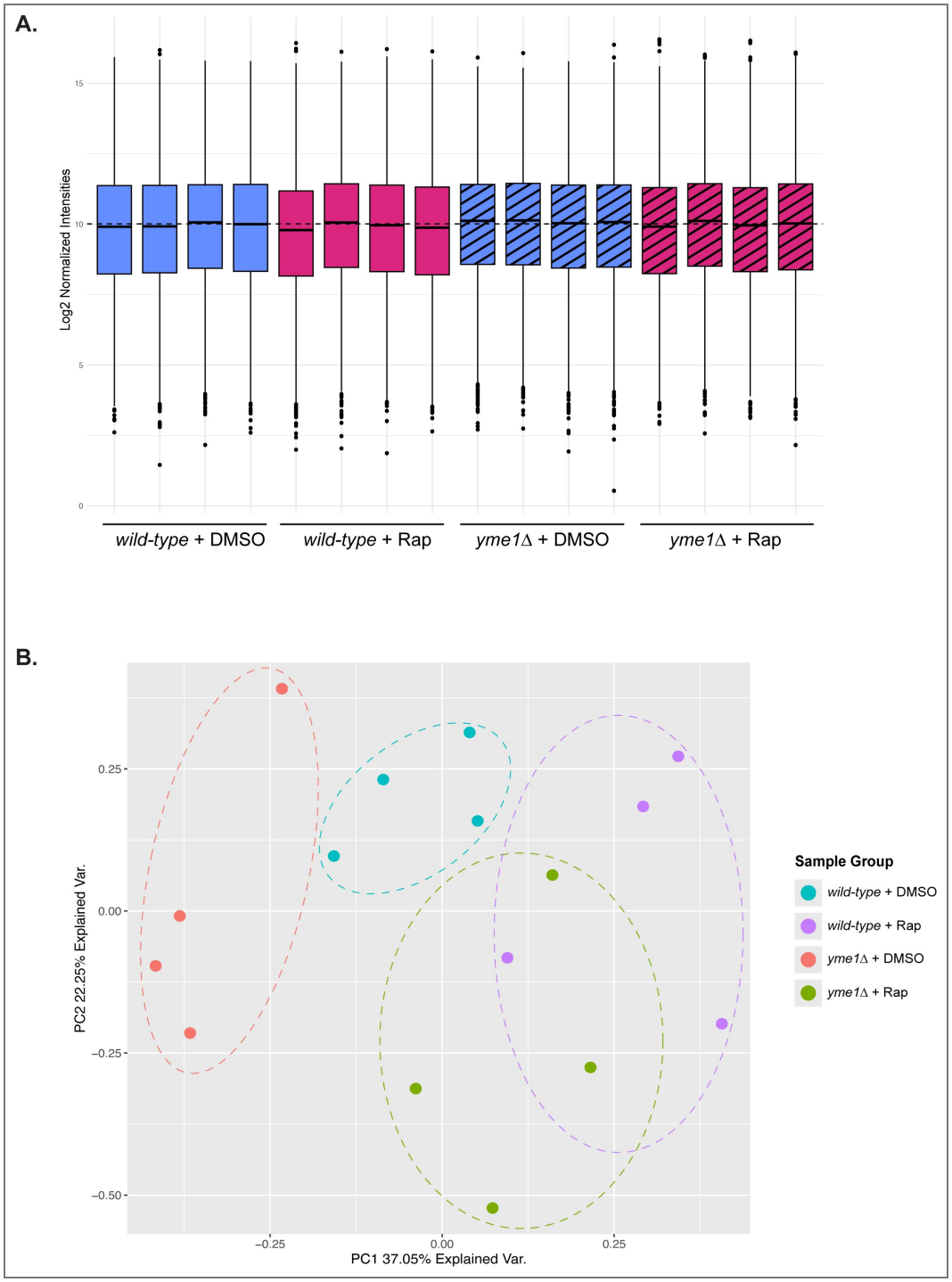

Figure S2. Mitoproteomics data quality control (Related to Figure 2).

(A) Box plot showing log2-normalized protein intensities between wild-type and *yme1Δ* cells treated with DMSO or Rap for 2 h (n = 4). Comparable distributions across conditions confirm successful data normalization. (B) Principal component analysis of proteome data from wild-type and *yme1Δ* cells treated with DMSO or Rap for 2 h (n = 4).

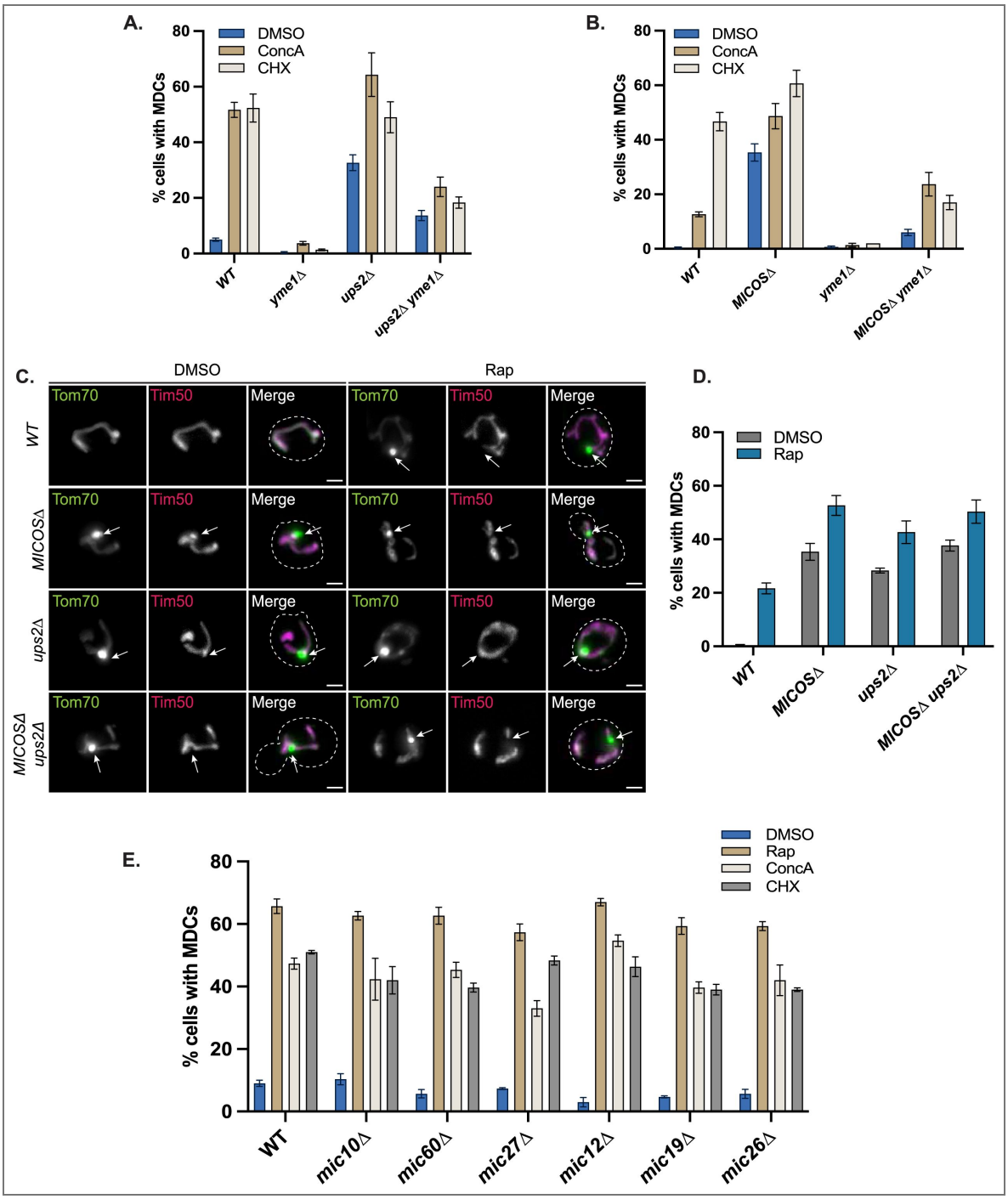

Figure S3. MDC assay profiling of Yme1-regulated factors (Related to Figures 3 & 4).

(A) Quantification of MDC formation in wild-type and indicated mutants treated with DMSO, ConcA, or CHX for 2 h. Error bars represent the mean ± SE of three replicates, *n* ≥ 100 cells per replicate. (B) Quantification of MDC formation in wild-type and indicated mutants treated with DMSO, ConcA, or CHX for 2 h. Error bars represent the mean ± SE of three replicates, *n* ≥ 100 cells per replicate. (C) Widefield images of wild-type and indicated mutants expressing Tom70-GFP and Tim50-mCherry treated with DMSO or Rap for 2 h. White arrows denote MDCs. Scale bar = 2 µm. (D) Quantification of (C) showing the percentage of cells with MDCs. Error bars represent the mean ± SE of three replicates, *n* ≥ 100 cells per replicate. (E) Quantification of MDC formation in wild-type and indicated mutants treated with DMSO, Rap, ConcA, or CHX for 2 h. Error bars represent the mean ± SE of three replicates, *n* ≥ 100 cells per replicate.

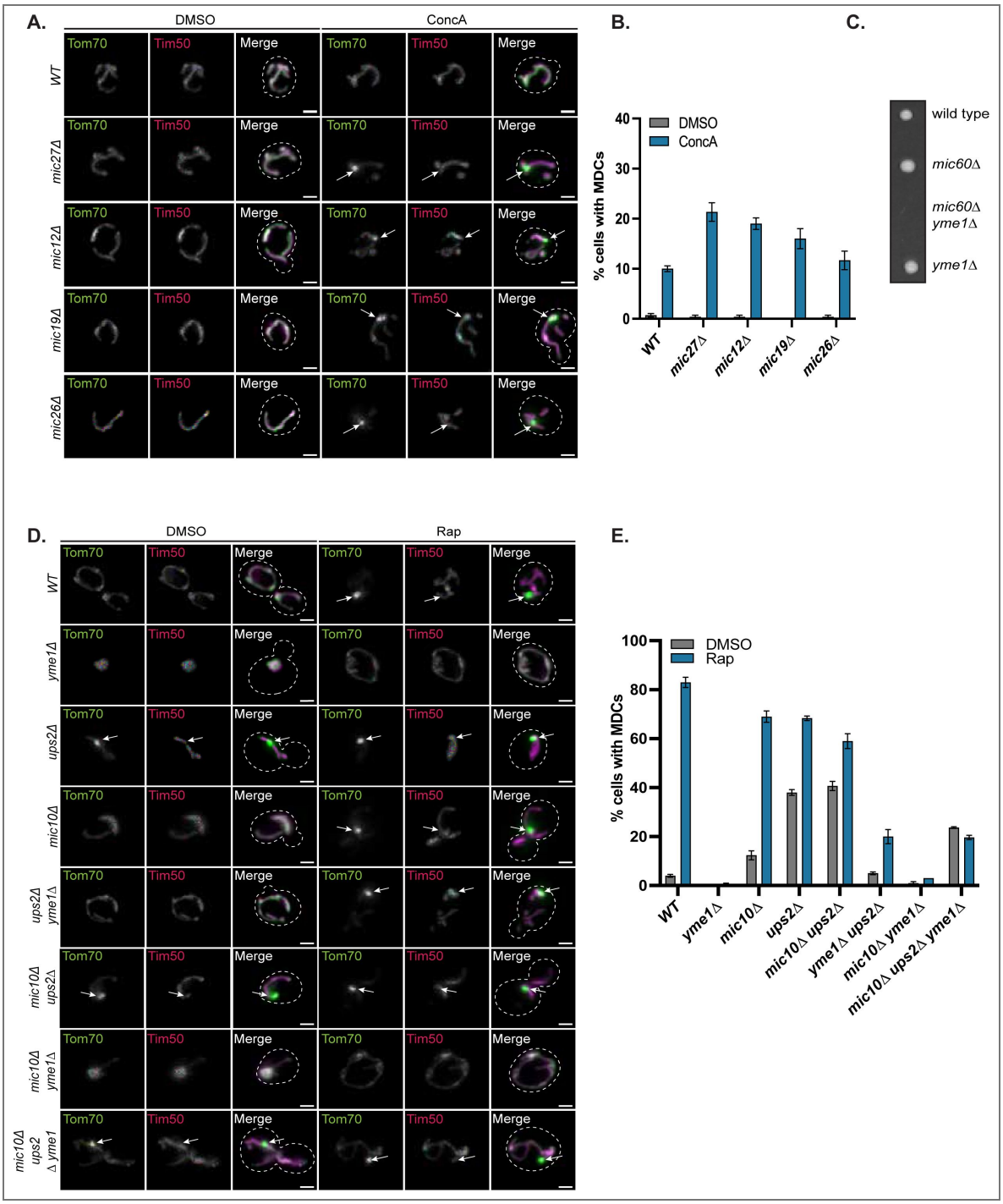

Figure S4. Role of the MICOS Complex in MDC formation: Effects of individual mutants and genetic interactions with Yme1, and Ups2 (Related to Figure 4).

(A) Widefield images of wild-type and indicated mutants expressing Tom70-GFP and Tim50-mCherry, grown in media containing low amino acids and treated with DMSO or ConcA for 2 h. White arrows denote MDCs. Scale bar = 2 μm. (B) Quantification of (A) showing the percentage of cells with MDCs. Error bars represent the mean ± SE of three replicates, $n \geq 100$ cells per replicate. (C) Tetrad dissection of *mic60Δ/+ yme1Δ/+* diploid cells demonstrating synthetic lethality between *MIC60* and *YME1*. (D) Widefield images of wild-type and indicated mutants expressing Tom70-GFP and Tim50-mCherry treated with DMSO or Rap for 2 h. White arrows denote MDCs. Scale bar = 2 μm. (E) Quantification of (D) showing the percentage of cells with MDCs. Error bars represent the mean ± SE of three replicates, $n \geq 100$ cells per replicate.

Data availability

The mass spectrometry proteomics data have been deposited to the ProteomeXchange Consortium via the PRIDE partner repository with the dataset identifier PXD075997. Source data for all figures and supporting files is available upon request.

Acknowledgements

We thank past and present members of the A.L. Hughes group for their discussion and manuscript comments. We thank members of Janet. M. Shaw laboratory for providing reagents, mitochondrial antibodies, and support early in the project. Proteomics analysis was conducted at the Thermo Fisher Scientific Center for Multiplexed Proteomics at Harvard Medical School. We thank Jonathan Van Vranken, PhD for performing the TMT-based proteomics experiments. We also thank Paul Stewart, PhD for his assistance with subsequent data analysis and visualizations. Lipidomics analysis was performed at the Metabolomics Core Facility at the University of Utah.

We sincerely thank John Alan Maschek, PhD for his expertise and assistance with the lipidomic analyses. Research was supported by National Institutes of Health grants GM119694 and AG061376 to A.L. Hughes and a University of Utah Graduate Research Fellowship to S.S. Balasubramaniam. J.F. is supported by NIH grant GM137894. The content is solely the responsibility of the authors and does not necessarily represent the official views of the NIH.

Additional information

Author contributions

Conceptualization, S.S. Balasubramaniam, J.R. Friedman, and A.L. Hughes; methodology, S.S. Balasubramaniam; formal analysis, S.S. Balasubramaniam; investigation, S.S. Balasubramaniam, A.E. Curtis; writing – original draft, S.S. Balasubramaniam; writing – review and editing, S.S. Balasubramaniam, J.R. Friedmann and A.L. Hughes; visualization, S.S. Balasubramaniam and A.L. Hughes; supervision, A.L. Hughes; funding acquisition, S.S. Balasubramaniam, J.R. Friedman, and A.L. Hughes.

Contact for reagent and resource sharing

Further information and requests for resources and reagents should be directed to and will be fulfilled by the Lead Contact, Adam Hughes. All unique/stable reagents generated in this study are available from the Lead Contact without restrictions.

Funding

Funder	Grant reference number	Author
HHS | NIH | National Institute of General Medical Sciences (NIGMS)	GM119694	Adam L Hughes
HHS | NIH | National Institute on Aging (NIA)	AG061376	Adam L Hughes
HHS | NIH | National Institute of General Medical Sciences (NIGMS)	GM137894	Jonathan Friedman

Author ORCID iDs

Sai Sangeetha Balasubramaniam: https://orcid.org/0000-0001-7524-0701
Jonathan R Friedman: https://orcid.org/0000-0001-8155-2429
Adam L Hughes: https://orcid.org/0000-0002-7095-3793

Additional files

Table S7

Table S6

Table S5

Table S4

Table S3

Table S2

Table S1

References

1. **Aaltonen MJ,** Friedman JR, Osman C, Salin B, Di Rago J-P, Nunnari J, Langer T, Tatsuta T (2016) MICOS and phospholipid transfer by Ups2–Mdm35 organize membrane lipid synthesis in mitochondria. *J Cell Biol* **213**:525-534 https://doi.org/10.1083/jcb.201602007 | PubMed
2. **Abeliovich H** (2023) Mitophagy in yeast: known unknowns and unknown unknowns. *Biochem J* **480**:1639-1657 https://doi.org/10.1042/bcj20230279 | PubMed
3. **Agrawal A,** Ramachandran R (2019) Exploring the links between lipid geometry and mitochondrial fission: Emerging concepts. *Mitochondrion* **49**:305-313 https://doi.org/10.1016/j.mito.2019.07.010 | PubMed
4. **Andersen EC** (2012) PCR-Directed In Vivo Plasmid Construction Using Homologous Recombination in Baker's Yeast. In: Orgogozo V, Rockman MV (Eds). *Molecular Methods for Evolutionary Genetics* NJ: Humana Press. pp. 409-421 https://doi.org/10.1007/978-1-61779-228-1_24 | PubMed
5. **Bahat A,** Gross A (2019) Mitochondrial plasticity in cell fate regulation. *J Biol Chem* **294**:13852-13863 https://doi.org/10.1074/jbc.rev118.000828 | PubMed
6. **Bähler J,** Wu J-Q, Longtine MS, Shah NG, Mckenzie Iii A, Steever AB, Wach A, Philippsen P, Pringle JR (1998) Heterologous modules for efficient and versatile PCR-based gene targeting in Schizosaccharomyces pombe. *Yeast* **14**:943-951 https://doi.org/10.1002/(sici)1097-0061(199807)14:10<943::aid-yea292>3.0.co;2-y | PubMed
7. **Brachmann C Baker,** Davies A, Cost GJ, Caputo E, Li J, Hieter P, Boeke JD (1998) Designer deletion strains derived from Saccharomyces cerevisiae S288C: A useful set of strains and plasmids for PCR-mediated gene disruption and other applications. *Yeast* **14**:115-132 https://doi.org/10.1002/(sici)1097-0061(19980130)14:2<115::aid-yea204>3.0.co;2-2 | PubMed
8. **Baker MJ,** Mooga VP, Guiard B, Langer T, Ryan MT, Stojanovski D (2012) Impaired Folding of the Mitochondrial Small TIM Chaperones Induces Clearance by the i-AAA Protease. *J Mol Biol* **424**:227-239 https://doi.org/10.1016/j.jmb.2012.09.019 | PubMed
9. **Bohnert M,** Zerbes RM, Davies KM, Mühleip AW, Rampelt H, Horvath SE, Boenke T, Kram A, Perschil I, Veenhuis M, *et al.* (2015) Central Role of Mic10 in the Mitochondrial Contact Site and Cristae Organizing System. *Cell Metab* **21**:747-755 https://doi.org/10.1016/j.cmet.2015.04.007 | PubMed
10. **Campbell CL,** Tanaka N, White KH, Thorsness PE (1994) Mitochondrial morphological and functional defects in yeast caused by yme1 are suppressed by mutation of a 26S protease subunit homologue. *Molecular biology of the cell* **5**:899-905 https://doi.org/10.1091/mbc.5.8.899 | PubMed
11. **Cogliati S,** Enriquez JA, Scorrano L (2016) Mitochondrial Cristae: Where Beauty Meets Functionality. *Trends Biochem Sci* **41**:261-273 https://doi.org/10.1016/j.tibs.2016.01.001 | PubMed
12. **Colina-Tenorio L,** Horten P, Pfanner N, Rampelt H (2020) Shaping the mitochondrial inner membrane in health and disease. *J Intern Med* **287**:645-664 https://doi.org/10.1111/joim.13031 | PubMed
13. **Connerth M,** Tatsuta T, Haag M, Klecker T, Westermann B, Langer T (2012) Intramitochondrial Transport of Phosphatidic Acid in Yeast by a Lipid Transfer Protein. *Science* **338**:815-818 https://doi.org/10.1126/science.1225625 | PubMed
14. **Deshwal S,** Fiedler KU, Langer T (2020) Mitochondrial Proteases: Multifaceted Regulators of Mitochondrial Plasticity. *Annu Rev Biochem* **89**:501-528 https://doi.org/10.1146/annurev-biochem-062917-012739 | PubMed

15. **Elias JE,** Gygi SP (2007) Target-decoy search strategy for increased confidence in large-scale protein identifications by mass spectrometry. *Nature methods* **4**:207-214 https://doi.org/10.1038/nmeth1019 | PubMed

16. **Eng JK,** Jahan TA, Hoopmann MR (2013) Comet: An open-source MS / MS sequence database search tool. *Proteomics* **13**:22-24 https://doi.org/10.1002/pmic.201200439 | PubMed

17. **English AM,** Schuler M-H, Xiao T, Kornmann B, Shaw JM, Hughes AL (2020) ER–mitochondria contacts promote mitochondrial-derived compartment biogenesis. *J Cell Biol* **219**:e202002144 https://doi.org/10.1083/jcb.202002144 | PubMed

18. **Francis BR,** Thorsness PE (2011) Hsp90 and mitochondrial proteases Yme1 and Yta10/12 participate in ATP synthase assembly in Saccharomyces cerevisiae. *Mitochondrion* **11**:587-600 https://doi.org/10.1016/j.mito.2011.03.008 | PubMed

19. **Friedman JR,** Mourier A, Yamada J, McCaffery JM, Nunnari J (2015) MICOS coordinates with respiratory complexes and lipids to establish mitochondrial inner membrane architecture. *eLife* **4**:e07739 https://doi.org/10.7554/eLife.07739 | PubMed

20. **Gu Z** (2022) Complex heatmap visualization. *iMeta* **1**:e43 https://doi.org/10.1002/imt2.43 | PubMed

21. **Gu Z,** Eils R, Schlesner M (2016) Complex heatmaps reveal patterns and correlations in multidimensional genomic data. *Bioinformatics* **32**:2847-2849 https://doi.org/10.1093/bioinformatics/btw313 | PubMed

22. **Hughes AL,** Gottschling DE (2012) An early age increase in vacuolar pH limits mitochondrial function and lifespan in yeast. *Nature* **492**:261-265 https://doi.org/10.1038/nature11654 | PubMed

23. **Hughes AL,** Hughes CE, Henderson KA, Yazvenko N, Gottschling DE (2016) Selective sorting and destruction of mitochondrial membrane proteins in aged yeast. *eLife* **5**:e13943 https://doi.org/10.7554/eLife.13943 | PubMed

24. **Hughes CS,** Moggridge S, Müller T, Sorensen PH, Morin GB, Krijgsveld J (2019) Single-pot, solid-phase-enhanced sample preparation for proteomics experiments. *Nat Protoc* **14**:68-85 https://doi.org/10.1038/s41596-018-0082-x | PubMed

25. **Huttlin EL,** Jedrychowski MP, Elias JE, Goswami T, Rad R, Beausoleil SA, Villén J, Haas W, Sowa ME, Gygi SP (2010) A Tissue-Specific Atlas of Mouse Protein Phosphorylation and Expression. *Cell* **143**:1174-1189 https://doi.org/10.1016/j.cell.2010.12.001 | PubMed

26. **Huynen MA,** Mühlmeister M, Gotthardt K, Guerrero-Castillo S, Brandt U (2016) Evolution and structural organization of the mitochondrial contact site (MICOS) complex and the mitochondrial intermembrane space bridging (MIB) complex. *Biochim Biophys Acta BBA - Mol Cell Res* **1863**:91-101 https://doi.org/10.1016/j.bbamcr.2015.10.009 | PubMed

27. **Kan KT,** Wilcock J, Lu H (2024) Role of Yme1 in mitochondrial protein homeostasis: from regulation of protein import, OXPHOS function to lipid synthesis and mitochondrial dynamics. *Biochem Soc Trans* **52**:1539-1548 https://doi.org/10.1042/bst20240450 | PubMed

28. **Klecker T,** Westermann B (2021) Pathways shaping the mitochondrial inner membrane. *Open Biol* **11**:210238 https://doi.org/10.1098/rsob.210238 | PubMed

29. **Koehler CM** (1998) Tim9p, an essential partner subunit of Tim10p for the import of mitochondrial carrier proteins. *EMBO J* **17**:6477-6486 https://doi.org/10.1093/emboj/17.22.6477 | PubMed

30. **Koehler CM,** Jarosch E, Tokatlidis K, Schmid K, Schweyen RJ, Schatz G (1998) Import of Mitochondrial Carriers Mediated by Essential Proteins of the Intermembrane Space. *Science* **279**:369-373 https://doi.org/10.1126/science.279.5349.369 | PubMed

31. **Koelmel JP,** Kroeger NM, Gill EL, Ulmer CZ, Bowden JA, Patterson RE, Yost RA, Garrett TJ (2017) Expanding Lipidome Coverage Using LC-MS/MS Data-Dependent Acquisition with Automated Exclusion List Generation. *J Am Soc Mass Spectrom* **28**:908-917 https://doi.org/10.1007/s13361-017-1608-0 | PubMed

32. **Kolberg L.,** Raudvere U., Kuzmin I., Vilo J., Peterson H (2020) gprofiler2 -- an R package for gene list functional enrichment analysis and namespace conversion toolset g:Profiler. *F1000Research* **9**:ELIXIR-709 https://doi.org/10.12688/f1000research.24956.2 | PubMed

33. **König T,** McBride HM (2024) Mitochondrial-derived vesicles in metabolism, disease, and aging. *Cell Metab* **36**:21-35 https://doi.org/10.1016/j.cmet.2023.11.014 | PubMed

34. **Körner C,** Barrera M, Dukanovic J, Eydt K, Harner M, Rabl R, Vogel F, Rapaport D, Neupert W, Reichert AS (2012) The C-terminal domain of Fcj1 is required for formation of crista junctions and interacts with the TOB/SAM complex in mitochondria. *Mol Biol Cell* **23**:2143-2155 https://doi.org/10.1091/mbc.e11-10-0831 | PubMed

35. **Leonhard K,** Stiegler A, Neupert W, Langer T (1999) Chaperone-like activity of the AAA domain of the yeast Yme1 AAA protease. *Nature* **398**:348-351 https://doi.org/10.1038/18704 | PubMed

36. **Li H,** Ruan Y, Zhang K, Jian F, Hu C, Miao L, Gong L, Sun L, Zhang X, Chen S, *et al.* (2016) Mic60/Mitofilin determines MICOS assembly essential for mitochondrial dynamics and mtDNA nucleoid organization. *Cell Death Differ* **23**:380-392 https://doi.org/10.1038/cdd.2015.102 | PubMed

37. **Li J,** Cai Z, Bomgarden RD, Pike I, Kuhn K, Rogers JC, Roberts TM, Gygi SP, Paulo JA (2021) TMTpro-18plex: The Expanded and Complete Set of TMTpro Reagents for Sample Multiplexing. *J Proteome Res* **20**:2964-2972 https://doi.org/10.1021/acs.jproteome.1c00168 | PubMed

38. **Li X,** Straub J, Medeiros TC, Mehra C, Den Brave F, Peker E, Atanassov I, Stillger K, Michaelis JB, Burbridge E, *et al.* (2022) Mitochondria shed their outer membrane in response to infection-induced stress. *Science* **375**:eabi4343 https://doi.org/10.1126/science.abi4343 | PubMed

39. **MacVicar T,** Ohba Y, Nolte H, Mayer FC, Tatsuta T, Sprenger H-G, Lindner B, Zhao Y, Li J, Bruns C, *et al.* (2019) Lipid signalling drives proteolytic rewiring of mitochondria by YME1L. *Nature* **575**:361-365 https://doi.org/10.1038/s41586-019-1738-6 | PubMed

40. **Matheson K,** Parsons L, Gammie A (2017) Whole-Genome Sequence and Variant Analysis of W303, a Widely-Used Strain of *Saccharomyces cerevisiae*. *G3 GenesGenomesGenetics* **7**:2219-2226 https://doi.org/10.1534/g3.117.040022 | PubMed

41. **Matyash V,** Liebisch G, Kurzchalia TV, Shevchenko A, Schwudke D (2008) Lipid extraction by methyl-tert-butyl ether for high-throughput lipidomics. *J Lipid Res* **49**:1137-1146 https://doi.org/10.1194/jlr.d700041-jlr200 | PubMed

42. **Mukherjee I,** Ghosh M, Meinecke M (2021) MICOS and the mitochondrial inner membrane morphology – when things get out of shape. *FEBS Lett* **595**:1159-1183 https://doi.org/10.1002/1873-3468.14089 | PubMed

43. **Mülleder M,** Capuano F, Pir P, Christen S, Sauer U, Oliver SG, Ralser M (2012) A prototrophic deletion mutant collection for yeast metabolomics and systems biology. *Nat Biotechnol* **30**:1176-1178 https://doi.org/10.1038/nbt.2442 | PubMed

44. **Navarrete-Perea J,** Yu Q, Gygi SP, Paulo JA (2018) Streamlined Tandem Mass Tag (SL-TMT) Protocol: An Efficient Strategy for Quantitative (Phospho)proteome Profiling Using Tandem Mass Tag-Synchronous Precursor Selection-MS3. *J Proteome Res* **17**:2226-2236 https://doi.org/10.1021/acs.jproteome.8b00217 | PubMed

45. **Ng MYW,** Wai T, Simonsen A (2021) Quality control of the mitochondrion. *Dev Cell* **56**:881-905 https://doi.org/10.1016/j.devcel.2021.02.009 | PubMed

46. **Ott C,** Ross K, Straub S, Thiede B, Götz M, Goosmann C, Krischke M, Mueller MJ, Krohne G, Rudel T, *et al.* (2012) Sam50 Functions in Mitochondrial Intermembrane Space Bridging and Biogenesis of Respiratory Complexes. *Mol Cell Biol* **32**:1173-1188 https://doi.org/10.1128/mcb.06388-11 | PubMed

47. **Perea V,** Cole C, Lebeau J, Dolina V, Baron KR, Madhavan A, Kelly JW, Grotjahn DA, Wiseman RL (2023) PERK signaling promotes mitochondrial elongation by remodeling membrane phosphatidic acid. *EMBO J* **42**:e113908 https://doi.org/10.15252/embj.2023113908 | PubMed

48. **Perez-Riverol Y,** Bandla C, Kundu DJ, Kamatchinathan S, Bai J, Hewapathirana S, John NS, Prakash A, Walzer M, Wang S, *et al.* (2025) The PRIDE database at 20 years: 2025 update. *Nucleic Acids Res* **53**:D543-D553 https://doi.org/10.1093/nar/gkae1011 | PubMed

49. **Pfanner N,** Warscheid B, Wiedemann N (2019) Mitochondrial proteins: from biogenesis to functional networks. *Nat Rev Mol Cell Biol* **20**:267-284 https://doi.org/10.1038/s41580-018-0092-0 | PubMed

50. **Picca A,** Guerra F, Calvani R, Coelho-Júnior HJ, Landi F, Bucci C, Marzetti E (2023) Mitochondrial-Derived Vesicles: The Good, the Bad, and the Ugly. *Int J Mol Sci* **24**:13835 https://doi.org/10.3390/ijms241813835 | PubMed

51. **Potting C,** Wilmes C, Engmann T, Osman C, Langer T (2010) Regulation of mitochondrial phospholipids by Ups1/PRELI-like proteins depends on proteolysis and Mdm35. *EMBO J* **29**:2888-2898 https://doi.org/10.1038/emboj.2010.169 | PubMed

52. **Rad R,** Li J, Mintseris J, O'Connell J, Gygi SP, Schweppe DK (2021) Improved Monoisotopic Mass Estimation for Deeper Proteome Coverage. *J Proteome Res* **20**:591-598 https://doi.org/10.1021/acs.jproteome.0c00563 | PubMed

53. **Raghuram N,** Hughes A (2024) Amino acids trigger MDC-dependent mitochondrial remodeling by altering mitochondrial function. *bioRxiv* https://doi.org/10.1101/2024.07.09.602707 | PubMed

54. **Schiller D** (2009) Pam17 and Tim44 act sequentially in protein import into the mitochondrial matrix. *Int J Biochem Cell Biol* **41**:2343-2349 https://doi.org/10.1016/j.biocel.2009.06.011 | PubMed

55. **Schreiner B,** Westerburg H, Forné I, Imhof A, Neupert W, Mokranjac D (2012) Role of the AAA protease Yme1 in folding of proteins in the intermembrane space of mitochondria. *Mol Biol Cell* **23**:4335-4346 https://doi.org/10.1091/mbc.e12-05-0420 | PubMed

56. **Schuler M-H,** English AM, VanderMeer L, Shaw JM, Hughes AL (2020) Amino Acids Promote Mitochondrial-Derived Compartment Formation in Mammalian Cells. *bioRxiv* https://doi.org/10.1101/2020.12.23.424218

57. **Schuler M-H,** English AM, Xiao T, Campbell TJ, Shaw JM, Hughes AL (2021) Mitochondrial-derived compartments facilitate cellular adaptation to amino acid stress. *Mol Cell* **81**:3786-3802. https://doi.org/10.1016/j.molcel.2021.08.021 | PubMed

58. **Schuster R,** Okamoto K (2022) An overview of the molecular mechanisms of mitophagy in yeast. *Biochim Biophys Acta BBA - Gen Subj* **1866**:130203 https://doi.org/10.1016/j.bbagen.2022.130203 | PubMed

59. **Schweppe DK,** Prasad S, Belford MW, Navarrete-Perea J, Bailey DJ, Huguet R, Jedrychowski MP, Rad R, McAlister G, Abbatiello SE, *et al.* (2019) Characterization and Optimization of Multiplexed Quantitative Analyses Using High-Field Asymmetric-Waveform Ion Mobility Mass Spectrometry. *Anal Chem* **91**:4010-4016 https://doi.org/10.1021/acs.analchem.8b05399 | PubMed

60. **Sheff MA,** Thorn KS (2004) Optimized cassettes for fluorescent protein tagging in *Saccharomyces cerevisiae*. *Yeast* **21**:661-670 https://doi.org/10.1002/yea.1130 | PubMed

61. **Sikorski RS,** Hieter P (1989) A System of Shuttle Vectors and Yeast Host Strains Designed for Efficient Manipulation of DNA in Saccharomyces cerevisiae. *Genetics* https://doi.org/10.1093/genetics/122.1.19 | PubMed

62. **Spiller MP,** Guo L, Wang Q, Tran P, Lu H (2015) Mitochondrial Tim9 protects Tim10 from degradation by the protease Yme1. *Biosci Rep* **35**:e00193 https://doi.org/10.1042/bsr20150038 | PubMed

63. **Storey JD,** Tibshirani R (2003) Statistical significance for genomewide studies. *Proc Natl Acad Sci* **100**:9440-9445 https://doi.org/10.1073/pnas.1530509100 | PubMed

64. **Sugiura A,** McLelland G, Fon EA, McBride HM (2014) A new pathway for mitochondrial quality control: mitochondrial-derived vesicles. *EMBO J* **33**:2142-2156 https://doi.org/10.15252/embj.201488104 | PubMed

65. **Suomalainen A,** Nunnari J (2024) Mitochondria at the crossroads of health and disease. *Cell* **187**:2601-2627 https://doi.org/10.1016/j.cell.2024.04.037 | PubMed

66. **Tamura Y,** Onguka O, Hobbs AEA, Jensen RE, Iijima M, Claypool SM, Sesaki H (2012) Role for Two Conserved Intermembrane Space Proteins, Ups1p and Up2p, in Intra-mitochondrial Phospholipid Trafficking. *J Biol Chem* **287**:15205-15218 https://doi.org/10.1074/jbc.m111.338665 | PubMed

67. **Tang J,** Zhang K, Dong J, Yan C, Hu C, Ji H, Chen L, Chen S, Zhao H, Song Z (2020) Sam50–Mic19–Mic60 axis determines mitochondrial cristae architecture by mediating mitochondrial outer and inner membrane contact. *Cell Death Differ* **27**:146-160 https://doi.org/10.1038/s41418-019-0345-2 | PubMed

68. **Tatsuta T,** Langer T (2017) Intramitochondrial phospholipid trafficking. *Biochim Biophys Acta BBA - Mol Cell Biol Lipids* **1862**:81-89 https://doi.org/10.1016/j.bbalip.2016.08.006 | PubMed

69. **Consortium The UniProt,** Bateman A, Martin M-J, Orchard S, Magrane M, Adesina A, Ahmad S, Bowler-Barnett EH, Bye-A-Jee H, Carpentier D, *et al.* (2025) UniProt: the Universal Protein Knowledgebase in 2025. *Nucleic Acids Res* **53**:D609-D617 https://doi.org/10.1093/nar/gkae1010 | PubMed

70. **Thorsness PE,** Fox TD (1993) Nuclear mutations in Saccharomyces cerevisiae that affect the escape of DNA from mitochondria to the nucleus. *Genetics* **134**:21-28 https://doi.org/10.1093/genetics/134.1.21 | PubMed

71. **Van Der Laan M,** Chacinska A, Lind M, Perschil I, Sickmann A, Meyer HE, Guiard B, Meisinger C, Pfanner N, Rehling P (2005) Pam17 Is Required for Architecture and Translocation Activity of the Mitochondrial Protein Import Motor. *Mol Cell Biol* **25**:7449-7458 https://doi.org/10.1128/mcb.25.17.7449-7458.2005 | PubMed

72. **Weber ER,** Hanekamp T, Thorsness PE (1996) Biochemical and functional analysis of the YME1 gene product, an ATP and zinc-dependent mitochondrial protease from S. cerevisiae. *Mol Biol Cell* **7**:307-317 https://doi.org/10.1091/mbc.7.2.307 | PubMed

73. **Wilson ZN,** Balasubramaniam SS, Wong S, Schuler M-H, Wopat MJ, Hughes AL (2024) Mitochondrial-derived compartments remove surplus proteins from the outer mitochondrial membrane. *J Cell Biol* **223**:e202307036 https://doi.org/10.1083/jcb.202307036 | PubMed

74. **Wilson ZN,** West M, English AM, Odorizzi G, Hughes AL (2024) Mitochondrial-Derived Compartments are multilamellar domains that encase membrane cargo and cytosol. *J Cell Biol* **223**:e202307035 https://doi.org/10.1083/jcb.202307035 | PubMed

75. **Wright K** (2025) nipals: Principal Components Analysis using NIPALS or Weighted EMPCA, with Gram-Schmidt Orthogonalization. R package version. version: v1.0 https://doi.org/10.32614/cran.package.nipals

76. **Xiao T,** English AM, Wilson ZN, Alan Maschek J, Cox JE, Hughes AL (2024) The phospholipids cardiolipin and phosphatidylethanolamine differentially regulate MDC biogenesis. *J Cell Biol* **223**:e202302069 https://doi.org/10.1083/jcb.202302069 | PubMed

77. **Yang Z,** Wang L, Yang C, Pu S, Guo Z, Wu Q, Zhou Z, Zhao H (2022) Mitochondrial Membrane Remodeling. *Front Bioeng Biotechnol* **9**:786806 https://doi.org/10.3389/fbioe.2021.786806 | PubMed

78. **Zerbes RM,** Bohnert M, Stroud DA, Von Der Malsburg K, Kram A, Oeljeklaus S, Warscheid B, Becker T, Wiedemann N, Veenhuis M, *et al.* (2012) Role of MINOS in Mitochondrial Membrane Architecture: Cristae Morphology and Outer Membrane Interactions Differentially Depend on Mitofilin Domains. *J Mol Biol* **422**:183-191 https://doi.org/10.1016/j.jmb.2012.05.004 | PubMed

Peer reviews

Reviewer #1 (Public review):

Summary:

In this manuscript, Balasubramaniam and colleagues continue this group's efforts to understand mitochondrial-derived compartments (MDCs) that bud off from yeast mitochondria in response to metabolic stress. In a previous genetic screen, they identified Ups lipid transfer proteins and the AAA-protease Yme1 as components that modulate MDC

formation. In this study, the authors link these observations by showing that Yme1 modulates levels of Ups1, Ups2, as well as MICOS complex members in the mitochondrial proteome. Using genetic approaches, they then show that Yme1's role on MDCs is dependent on its catalytic activity (via an inactive mutant) and that YME1 shows genetic interactions with UPS1/2 and MIC10/MIC60. The overall model is that Yme1 activity responds to metabolic cues and acts via proteolysis of these two distinct mitochondrial machineries to regulate MDC biogenesis.

Strengths:

The strengths of the study are its integration of mitochondrial proteomics with strong genetic approaches, as well as synergy with the authors' previous studies on the role of lipids in MD genesis. The work is overall well carried-out and experiments are thoughtfully discussed.

Weaknesses:

The major weaknesses are a lack of mechanistic resolution surrounding the model, e.g., proposed or tested mechanisms by which Yme1 activity is regulated by metabolic cues, or how Ups1/2 activity and the MICOS contribute to MDC generation. The authors acknowledge these as open questions, but addressing them would still enhance the significance of the study.

https://doi.org/10.7554/eLife.111713.1.sa3

Reviewer #2 (Public review):

In this manuscript, the authors report a novel regulation of the outer mitochondrial membrane remodeling domains called mitochondria-derived compartments, MDCs. The team has previously established the main principles behind this recently identified quality control pathway, but the mechanisms that control MDCs formation remain incompletely understood. Using the baker's yeast model, the authors identify the conserved mitochondrial protease Yme1 as a crucial factor that regulates MDC formation. Mechanistically, Yme1's proteolytic function controls the levels of Ups1 and Ups2 lipid transfer proteins and the components of the membrane organizing complex called MICOS, thus providing a plausible model as to how Yme1-dependent proteolysis permits MDC formation through the removal of lipid and MICOS-dependent constraints. Finally, the authors show that this Yme1-mediated activity is also defined by metabolic conditions. In principle, this study is interesting and novel, and holds potential to provide new insights into the regulation of the MDC pathway that emerged as a new fundamental mitochondrial quality control mechanism. However, the following points should be carefully addressed.

Major points:

(1) Yme1 has been previously shown to regulate mitochondria-specific autophagy through Atg32 processing. Given the high similarity of the MDC pathway to piecemeal autophagy and the fact that both pathways share some of the core components, the authors should address the involvement of Atg32 in their model. It would also be important to include a brief discussion addressing the differences between piecemeal autophagy and the MDC pathway.

(2) The Rpt3 (P215L) expression experiment is interesting, but appears to be somewhat superficial due to the unclear mechanism by which the mitochondrial network morphology is restored in these cells. Could this result be replicated in the dnm1Δ mgm1Δ double deletion mutant, which is a well-established model for mitochondrial network restoration?

(3) Figure 3E. The changes in PE levels appear to be minor. While statistically significant, the observed differences may not be physiologically relevant. More in-depth lipidomic analysis

data should be presented to substantiate the authors' argument and better address the questions at hand. Related to that, could PE or PA supplementation stimulate MDC formation?

(4) The connection between rapamycin treatment and Yme1-regulated MDC formation is unclear and puzzling and needs to be explained better.

(5) The MICOS complex is clearly involved in the regulation of MDC, but the manuscript misses the mark on providing compelling evidence and a clear explanation as to how MICOS contributes to said regulation.

Minor points:

(1) The authors should discuss potential reasons for the dramatically different rates of MDC formation in the S288C and W303 background cells. Does this have anything to do with generally more robust mitochondrial functions in the latter cells?

(2) Proper statistical analyses should be provided for all the graphs presented.

(3) The authors should include Yme1 immunoblots to confirm the identity of strains being studied and validate the presence or overexpression of Yme1 and its catalytic mutant in their experiments.

https://doi.org/10.7554/eLife.111713.1.sa2

Reviewer #3 (Public review):

Summary:

Since describing MDCs over a decade ago, the lab of the corresponding author, Hughes, has been at the forefront of further characterizing these structures. Here, they follow up on recent work (PMID: 38497895), where a screen identified Yme1 as a potential regulator of MDCs. After confirming that Yme1-ko prevents MDCs that are usually induced via various established treatments (Rapamycin, cycloheximide, Concanavalin A), the authors confirmed that the proteolytic activity of Yme1 is required. Next, using proteomics, they identified how loss of Yme1 impacts the mitochondrial proteome with and without Rapamycin treatment to induce MDCs. From this result and based on insight from other published data implicating lipids, the focused initially on the lipid transfer protein Usp2, a known target of Yme1. Here, they showed that loss of Usp2 could partially rescue MDC formation in Yme1-ko cells. To look for other Yme1 targets that might also be involved in MDC formation, next, they investigated the MICOS complex, which was also notable in their proteomics data. They then showed that inhibiting MICOS also partially restored MDC formation in Yme1-ko cells. They then tested the combined effects of Usp2 and MDC inhibition on MDCs, which was limited by the fact that the combination of full MICOS disruption, Usp2-KO, and Yme1-KO was not viable. To circumvent this limitation, they investigated the knockout of individual MICOS subunits in combination with Usp2 and/or Yme1. Finally, they showed that growth conditions also mediate MDC formation in the context of Yme1 overexpression. In rich media, Yme1 overexpression induces MDCs on its own. However, this induction is lost upon amino acid starvation, suggesting that there are still other as-yet-unidentified factors regulating the formation of MDCs.

Strengths:

The authors use unbiased approaches and genetic models to begin unraveling a novel regulatory role of Yme1 in the formation of MDCs.

Weaknesses:

(1) The authors find both Ups1 and Ups2 in their screens, but only focus on Ups2 in this paper. It would be good to know why they did not also investigate Ups1, and its other protease Atp23, which could potentially act similarly to Yme1, or even rescue the loss of Yme1.

(2) I'm not convinced that the data support the notion that Usp2 and MICOS have distinct effects on MDCs. In Figure S3C-D, there is no statistical analysis to indicate whether the small differences between the MICOS-ko and the double knockout are significant. If MICOS-ko and Ups2-ko were acting through different mechanisms, one would expect their combination to be additive; this does not appear to be the case, as both single deletions and the double deletion all cause similar levels of MDCs (~30-40%). Rather, this result is what you would expect if they were working through the same mechanism. There also does not appear to be an additive effect in Figure 4F-G, when using the mic60-ko rather than the complete MICOS-ko. In this regard, the authors note in their discussion that 'loss of MICOS may disrupt membrane associations or alter lipid distribution between mitochondrial subcompartments' (lines 390-392). The latter situation seems like it would be the same mechanism as Usp2 and would more accurately explain their findings.

(3) The manuscript is missing key data confirming the re-expression or overexpression of Yme1 protein (Figure 1 E/G and Figure 5A). It is important to know the relative levels of expression of the re-expressed proteins to each other and to endogenous Yme1.

(4) Some clarification of the details for metabolically restrictive conditions would be helpful.

(5) Beyond just the presence/absence of MDCs, does more detailed quantification of their size/shape reveal any subtle differences between conditions?

https://doi.org/10.7554/eLife.111713.1.sa1

Author response:

We thank the editors and reviewers for their thoughtful and constructive evaluation of our manuscript. We are pleased that the reviewers found the study valuable and the evidence supporting a role for Yme1 in MDC formation solid. As described below, we plan to modify the manuscript to clarify the lipid model, better explain the relationship between Ups-family proteins and MICOS, distinguish MDC formation from Atg32-dependent mitophagy, clarify metabolic conditions, add statistical analyses where missing, and strengthen Yme1 validation with immunoblotting.

> ***eLife Assessment***
>
> *This valuable study demonstrates that the inner membrane protease YME1 contributes to the formation of mitochondrial-derived compartments in yeast through the modulation of both the lipid transporter UPS2 and the MICOS complex. The evidence supporting this model is solid, although this manuscript could be improved by providing additional evidence supporting the independent roles for UPS2 and MICOS regulation in this process. This work will be of interest to cell biologists, biochemists, and geneticists interested in understanding the molecular basis of mitochondrial regulation and function.*

We appreciate this positive assessment and agree that the roles of Ups-family lipid transport and MICOS in MDC regulation could be expanded further. This will be an important topic for future studies, especially with regard to how MICOS contributes to MDC formation. In the current revision, we will add new genetic data focused on PA-linked lipid metabolism through the yeast Pah1/Lipin pathway, which we think will help strengthen and clarify the lipid arm of the model. Our current interpretation is that Yme1-regulated Ups-family lipid

transport and MICOS may both influence a shared mitochondrial membrane state that permits MDC formation. This interpretation is consistent with our genetic data and with known connections between Ups proteins, MICOS, and mitochondrial membrane organization.

> ***Reviewer #1 (Public review):***
>
> *Summary:*
>
> *In this manuscript, Balasubramaniam and colleagues continue this group's efforts to understand mitochondrial-derived compartments (MDCs) that bud off from yeast mitochondria in response to metabolic stress. In a previous genetic screen, they identified Ups lipid transfer proteins and the AAA-protease Yme1 as components that modulate MDC formation. In this study, the authors link these observations by showing that Yme1 modulates levels of Ups1, Ups2, as well as MICOS complex members in the mitochondrial proteome. Using genetic approaches, they then show that Yme1's role on MDCs is dependent on its catalytic activity (via an inactive mutant) and that YME1 shows genetic interactions with UPS1/2 and MIC10/MIC60. The overall model is that Yme1 activity responds to metabolic cues and acts via proteolysis of these two distinct mitochondrial machineries to regulate MDC biogenesis.*
>
> *Strengths:*
>
> *The strengths of the study are its integration of mitochondrial proteomics with strong genetic approaches, as well as synergy with the authors' previous studies on the role of lipids in MD genesis. The work is overall well carried-out and experiments are thoughtfully discussed.*
>
> *Weaknesses:*
>
> *The major weaknesses are a lack of mechanistic resolution surrounding the model, e.g., proposed or tested mechanisms by which Yme1 activity is regulated by metabolic cues, or how Ups1/2 activity and the MICOS contribute to MDC generation. The authors acknowledge these as open questions, but addressing them would still enhance the significance of the study.*

We thank the reviewer for the positive assessment, and we agree that the upstream regulation of this response remains an important open question. Yme1-dependent MDC regulation could involve changes in Yme1 activity, substrate accessibility, or broader changes in mitochondrial lipid and protein organization. Fully resolving how metabolic state gates this response will require future work, likely outside the scope of the current study.

We also agree that the manuscript would benefit from a more developed discussion of how lipid changes could contribute to MDC formation. Our prior work showed that reduced mitochondrial PE promotes MDC formation, whereas cardiolipin is required for MDC biogenesis (Xiao et al., 2024). We proposed that reduced PE changes the membrane environment of mitochondrial outer membrane proteins, potentially affecting their stability, abundance, insertion, or lateral organization within the membrane. Such changes could increase the pool of proteins available for sorting into MDCs or make the outer membrane more permissive for domain formation. In the revision, we will connect this model more directly to Yme1-dependent regulation of Ups-family lipid transport.

We will also expand the model to incorporate PA-linked metabolism. We did not initially focus heavily on Ups1 because complete loss of UPS1, or loss of downstream cardiolipin synthesis through CRD1, blocks MDC formation because cardiolipin is required. Thus, complete disruption of Ups1-dependent lipid transport may obscure the effects of more moderate changes in PA flux. To address this, we will include additional lipid measurements

and new genetic data targeting PA metabolism through the yeast Pah1/Lipin pathway. Because Pah1 converts PA to DAG, this provides a way to alter PA-linked metabolism without simply eliminating cardiolipin synthesis. Our new data suggest that PA accumulation or altered PA-linked lipid flux may also promote MDC formation. Together, these findings support a broader model in which reduced PE and increased PA alter both the organization of OMM proteins and the physical properties of the membrane, including curvature and domain formation, thereby creating a membrane state that is more permissive for MDC biogenesis.

> ***Reviewer #2 (Public review):***
>
> *In this manuscript, the authors report a novel regulation of the outer mitochondrial membrane remodeling domains called mitochondria-derived compartments, MDCs. The team has previously established the main principles behind this recently identified quality control pathway, but the mechanisms that control MDCs formation remain incompletely understood. Using the baker's yeast model, the authors identify the conserved mitochondrial protease Yme1 as a crucial factor that regulates MDC formation. Mechanistically, Yme1's proteolytic function controls the levels of Ups1 and Ups2 lipid transfer proteins and the components of the membrane organizing complex called MICOS, thus providing a plausible model as to how Yme1-dependent proteolysis permits MDC formation through the removal of lipid and MICOS-dependent constraints. Finally, the authors show that this Yme1-mediated activity is also defined by metabolic conditions. In principle, this study is interesting and novel, and holds potential to provide new insights into the regulation of the MDC pathway that emerged as a new fundamental mitochondrial quality control mechanism. However, the following points should be carefully addressed.*
>
> *Major points:*
>
> *(1) Yme1 has been previously shown to regulate mitochondria-specific autophagy through Atg32 processing. Given the high similarity of the MDC pathway to piecemeal autophagy and the fact that both pathways share some of the core components, the authors should address the involvement of Atg32 in their model. It would also be important to include a brief discussion addressing the differences between piecemeal autophagy and the MDC pathway.*

We agree that this is an important point. The reason we did not focus on Atg32 in the current manuscript is that we previously investigated the relationship between MDC formation and Atg32-dependent mitophagy and found that Atg32 is dispensable for MDC formation (Hughes et al., 2016). Based on that result, we do not anticipate that Atg32 is required for the Yme1-dependent MDC phenotypes described here. This is also consistent with the different growth conditions associated with these pathways: Atg32-dependent mitophagy is stimulated under respiratory or post-diauxic conditions, whereas MDCs do not form under the respiratory conditions that stimulate Atg32-dependent mitophagy (Hughes et al., 2016; Raghuram and Hughes, 2024).

We will clarify this distinction in the revised manuscript. In addition, to be thorough, we plan to generate and test the Atg32-GFP variant previously shown to block Yme1-dependent Atg32 processing and mitophagy (Wang et al., 2013). This will allow us to test directly whether preventing Yme1-dependent Atg32 cleavage affects MDC formation. If successful and interpretable, we will include these data in the revised manuscript.

> *(2) The Rpt3 (P215L) expression experiment is interesting, but appears to be somewhat superficial due to the unclear mechanism by which the mitochondrial network morphology is restored in these cells. Could this result be replicated in the dnm1Δ*

> *mgm1Δ double deletion mutant, which is a well-established model for mitochondrial network restoration?*

We agree that the Rpt3(P215L) experiment is best viewed as a morphology control. The purpose was to test whether abnormal mitochondrial morphology alone explains the MDC defect in yme1Δ cells. Because Rpt3(P215L) improved mitochondrial morphology but did not restore MDC formation, we interpret this as evidence that morphology alone is not sufficient.

We attempted to generate the requested dnm1Δ mgm1Δ yme1Δ triple-mutant combination, but that strain combination has not been viable in our hands. However, we do have dnm1Δ data showing that altering mitochondrial structure can rescue some morphological features but does not restore MDC formation in yme1Δ cells. We will include these data where appropriate and clarify that this experiment is intended as a morphology control.

> *(3) Figure 3E. The changes in PE levels appear to be minor. While statistically significant, the observed differences may not be physiologically relevant. More in-depth lipidomic analysis data should be presented to substantiate the authors' argument and better address the questions at hand. Related to that, could PE or PA supplementation stimulate MDC formation?*

We agree that additional lipid data would strengthen this part of the manuscript. We initially streamlined the lipid section because we had previously examined the lipid requirements for MDC formation in detail, showing that reduced mitochondrial PE can promote MDC formation, whereas cardiolipin is required (Xiao et al., 2024). However, the current study would benefit from a broader analysis of the lipid changes associated with Yme1-dependent regulation.

In the revision, we will expand the lipid data to include additional lipid species and incorporate these results into the model. We will also add new genetic data targeting PA metabolism through the yeast Pah1/Lipin pathway. Together, these data suggest that PA accumulation or altered PA-linked lipid flux may also contribute to MDC formation. This supports a broader lipid-balance or lipid-shunting model in which reduced PE, increased PA, or altered lipid distribution between mitochondrial membranes could influence OMM remodeling through effects on membrane curvature, OMM protein organization, or mitochondrial membrane contacts.

We agree that direct PE or PA supplementation would be a valuable experiment. We have attempted lipid supplementation but have not been able to deliver these lipids effectively to yeast cells in a way that produces interpretable results. We are therefore focusing on lipid profiling and genetic approaches that alter lipid metabolism inside the cell.

> *(4) The connection between rapamycin treatment and Yme1-regulated MDC formation is unclear and puzzling and needs to be explained better.*

We agree that this connection is not fully clear. In this manuscript, rapamycin is used primarily as a robust MDC-inducing condition. Our data do not define the full pathway connecting TORC1 inhibition to Yme1-dependent mitochondrial remodeling.

In the revision, we will either clarify this point or reduce the emphasis on rapamycin as a mechanistic entry point. Our current interpretation is that rapamycin creates a metabolic/mitochondrial state in which Yme1-dependent remodeling of lipid and membrane-organization pathways becomes important for MDC formation. Whether this involves direct regulation of Yme1, altered substrate availability, altered membrane composition, or a combination of these remains open.

> *(5) The MICOS complex is clearly involved in the regulation of MDC, but the manuscript misses the mark on providing compelling evidence and a clear explanation as to how*

> *MICOS contributes to said regulation.*

We agree that the mechanism by which MICOS regulates MDC formation remains an important open question and will be a major focus of future work. Our current data show that MICOS perturbation can partially restore MDC formation in yme1Δ cells, supporting a role for MICOS in this pathway. This analysis was motivated in part by the incomplete genetic suppression achieved through the lipid pathway alone, which suggested that additional Yme1-regulated factors contribute to MDC formation.

MICOS therefore represents a strong candidate for this additional regulatory input. However, defining whether MICOS acts through lipid distribution, OMM-IMM organization, membrane architecture, or another mechanism will require a deeper investigation than is possible within the scope of the current study. We will clarify this point in the revised manuscript and present the current findings as the beginning of a broader investigation into how MICOS contributes to MDC biogenesis.

> *Minor points:*
>
> *(1) The authors should discuss potential reasons for the dramatically different rates of MDC formation in the S288C and W303 background cells. Does this have anything to do with generally more robust mitochondrial functions in the latter cells?*

We agree this is worth discussing. One likely explanation is that the difference reflects broader differences in mitochondrial activity and metabolic state between these strain backgrounds. We and others have shown that W303 cells have more robust respiratory mitochondrial function than BY/S288C-derived cells, and in our hands W303 also shows lower MDC formation. This fits our broader model that MDCs are favored in glucose-grown or metabolically perturbed cells and do not form under respiratory conditions (Raghuram and Hughes, 2024). We do not yet know the genetic basis for this difference, so we will present this as an interesting future direction.

> *(2) Proper statistical analyses should be provided for all the graphs presented.*

We will add statistical analyses where missing.

> *(3) The authors should include Yme1 immunoblots to confirm the identity of strains being studied and validate the presence or overexpression of Yme1 and its catalytic mutant in their experiments.*

We agree that direct validation of Yme1 protein levels will strengthen the manuscript. Our quantitative mitochondrial proteomics already confirms strong depletion of Yme1 in yme1Δ cells, and we will also include quantitative proteomics showing increased Yme1 abundance in the overexpression strain. In addition, we have now obtained a Yme1 antibody from a colleague and will include immunoblots validating Yme1 loss, re-expression, catalytic mutant expression, and overexpression where appropriate.

> ***Reviewer #3 (Public review):***
>
> *Summary:*
>
> *Since describing MDCs over a decade ago, the lab of the corresponding author, Hughes, has been at the forefront of further characterizing these structures. Here, they follow up on recent work (PMID: 38497895), where a screen identified Yme1 as a potential regulator of MDCs. After confirming that Yme1-ko prevents MDCs that are usually induced via various established treatments (Rapamycin, cycloheximide, Concanavalin A), the authors confirmed that the proteolytic activity of Yme1 is required. Next, using proteomics, they identified how loss of Yme1 impacts the mitochondrial proteome with and without Rapamycin treatment to induce MDCs. From this result and based on insight*

> *from other published data implicating lipids, the focused initially on the lipid transfer protein Usp2, a known target of Yme1. Here, they showed that loss of Usp2 could partially rescue MDC formation in Yme1-ko cells. To look for other Yme1 targets that might also be involved in MDC formation, next, they investigated the MICOS complex, which was also notable in their proteomics data. They then showed that inhibiting MICOS also partially restored MDC formation in Yme1-ko cells. They then tested the combined effects of Usp2 and MDC inhibition on MDCs, which was limited by the fact that the combination of full MICOS disruption, Usp2-KO, and Yme1-KO was not viable. To circumvent this limitation, they investigated the knockout of individual MICOS subunits in combination with Usp2 and/or Yme1. Finally, they showed that growth conditions also mediate MDC formation in the context of Yme1 overexpression. In rich media, Yme1 overexpression induces MDCs on its own. However, this induction is lost upon amino acid starvation, suggesting that there are still other as-yet-unidentified factors regulating the formation of MDCs.*
>
> *Strengths:*
>
> *The authors use unbiased approaches and genetic models to begin unraveling a novel regulatory role of Yme1 in the formation of MDCs.*
>
> *Weaknesses:*
>
> *(1) The authors find both Ups1 and Ups2 in their screens, but only focus on Ups2 in this paper. It would be good to know why they did not also investigate Ups1, and its other protease Atp23, which could potentially act similarly to Yme1, or even rescue the loss of Yme1.*

We agree that Ups1 and Atp23 are important to consider. We initially focused on Ups2 because its deletion partially restores MDC formation in yme1Δ cells and because of its connection to mitochondrial PE synthesis, which we had previously shown to regulate MDC formation (Xiao et al., 2024). Ups1 is more difficult to assess genetically because complete loss of UPS1, or of downstream cardiolipin synthesis through CRD1, blocks MDC formation due to the requirement for cardiolipin. Thus, an ups1Δ phenotype cannot readily reveal whether a more moderate reduction in Ups1 activity, and the resulting accumulation or redistribution of PA, might promote MDC formation.

In the revision, we will explain this rationale and include new genetic data targeting PA metabolism through the yeast Pah1/Lipin pathway. This provides a way to test the contribution of PA accumulation without simultaneously eliminating cardiolipin synthesis, and our initial results support a role for PA-linked lipid remodeling in partially bypassing the requirement for Yme1. We will also discuss Atp23 as a potentially important regulator of Ups1 and PA metabolism. A full investigation of Atp23 will be an important direction for future work.

> *(2) I'm not convinced that the data support the notion that Usp2 and MICOS have distinct effects on MDCs. In Figure S3C-D, there is no statistical analysis to indicate whether the small differences between the MICOS-ko and the double knockout are significant. If MICOS-ko and Ups2-ko were acting through different mechanisms, one would expect their combination to be additive; this does not appear to be the case, as both single deletions and the double deletion all cause similar levels of MDCs (~30-40%). Rather, this result is what you would expect if they were working through the same mechanism. There also does not appear to be an additive effect in Figure 4F-G, when using the mic60-ko rather than the complete MICOS-ko. In this regard, the authors note in their discussion that 'loss of MICOS may disrupt membrane associations or alter lipid distribution between mitochondrial subcompartments' (lines 390-392). The latter*

> *situation seems like it would be the same mechanism as Usp2 and would more accurately explain their findings.*

This is a very good point, and we agree with the reviewer's interpretation. The lack of strong additivity is consistent with Ups2 and MICOS acting within the same pathway or converging on a shared mechanism, rather than representing two separate mechanisms of MDC regulation. We did not intend to imply that these must be independent pathways. In the revised manuscript, we will ensure that the text reflects this interpretation and will add statistical analyses to the relevant comparisons.

> *(3) The manuscript is missing key data confirming the re-expression or overexpression of Yme1 protein (Figure 1 E/G and Figure 5A). It is important to know the relative levels of expression of the re-expressed proteins to each other and to endogenous Yme1.*

We agree that direct validation of Yme1 protein levels is important. Our quantitative mitochondrial proteomics already confirms strong depletion of Yme1 in yme1Δ cells, and we will also include quantitative proteomics showing increased Yme1 abundance in the overexpression strain. In addition, we have now obtained a Yme1 antibody from a colleague and will add immunoblots validating Yme1 loss, re-expression, catalytic mutant expression, and overexpression.

> *(4) Some clarification of the details for metabolically restrictive conditions would be helpful.*

Thanks for this suggestion. We will clarify these conditions throughout the manuscript and figure legends and will define exactly what we mean by low-amino-acid, amino-acid-free, synthetic, and rich media conditions. More broadly, MDC formation is strongly influenced by media composition and mitochondrial metabolic state. MDCs form less efficiently in synthetic media and do not form under conditions that promote respiratory mitochondrial function (Raghuram and Hughes, 2024).

> *(5) Beyond just the presence/absence of MDCs, does more detailed quantification of their size/shape reveal any subtle differences between conditions?*

This is an interesting question. In our hands, MDC size and shape are variable and appear strongly influenced by mitochondrial fission/fusion state. Conditions that favor more fused mitochondrial networks can produce larger MDC-like structures, whereas fragmented networks can produce smaller structures. So far, we have not found a simple size or shape metric that explains the Yme1/Ups2/MICOS phenotypes better than MDC frequency.

We will clarify this point in the revised manuscript and avoid implying that MDC frequency captures every possible morphological difference. More detailed morphometric analysis of MDC size, topology, and maturation state will be an important future direction, especially as we connect lipid remodeling to membrane curvature and MDC biogenesis.

References

Hughes, A.L., Hughes, C.E., Henderson, K.A., Yazvenko, N., and Gottschling, D.E. 2016. Selective sorting and destruction of mitochondrial membrane proteins in aged yeast. eLife. 5. doi: 10.7554/eLife.13943.

Raghuram, N., and Hughes, A.L. 2024. Amino acids trigger MDC-dependent mitochondrial remodeling by altering mitochondrial function. bioRxiv. 2024.07.09.602707. doi: 10.1101/2024.07.09.602707.

Wang, K., Jin, M., Liu, X., and Klionsky, D.J. 2013. Proteolytic processing of Atg32 by the mitochondrial i-AAA protease Yme1 regulates mitophagy. Autophagy. 9(11):1828–1836. doi: 10.4161/auto.26281.

Xiao, T., English, A.M., Wilson, Z.N., Maschek, J.A., Cox, J.E., and Hughes, A.L. 2024. The phospholipids cardiolipin and phosphatidylethanolamine differentially regulate MDC biogenesis. Journal of Cell Biology. 223(5). doi: 10.1083/jcb.202302069.

https://doi.org/10.7554/eLife.111713.1.sa0